Mapping the multi-decadal mangrove dynamics of the Australian coastline

Lymburner, Leo; Bunting, Pete; Lucas, Richard; Scarth, Peter; Alam, Imam; Phillips, Claire; Ticehurst, Catherine; Held, Alex

Published in:
Remote Sensing of Environment

DOI:
10.1016/j.rse.2019.05.004

Publication date:
2019

Citation for published version (APA):
Lymburner, L., Bunting, P., Lucas, R., Scarth, P., Alam, I., Phillips, C., Ticehurst, C., & Held, A. (2019). Mapping the multi-decadal mangrove dynamics of the Australian coastline. *Remote Sensing of Environment*. https://doi.org/10.1016/j.rse.2019.05.004

Remote Sensing of Environment xxx (xxxx) xxxx

Contents lists available at ScienceDirect

Remote Sensing of Environment

journal homepage: www.elsevier.com/locate/rse

Mapping the multi-decadal mangrove dynamics of the Australian coastline

Leo Lymburner[a,*], Peter Bunting[b], Richard Lucas[b], Peter Scarth[c], Imam Alam[a], Claire Phillips[a], Catherine Ticehurst[d], Alex Held[d]

[a] National Earth and Marine Observation Group, Geoscience Australia, Symonston, ACT, Australia
[b] Earth Observation and Ecosystem Dynamics Research Group, Department of Geography and Earth Sciences, Aberystwyth University, Aberystwyth, United Kingdom
[c] Joint Remote Sensing Research Program, School of Environment and Earth Sciences, University of Queensland, Brisbane, Queensland 4067, Australia
[d] CSIRO, Land and Water Business Unit, Black Mountain Laboratories, Australian Capital Territory, Australia

ARTICLE INFO

Keywords:
Mangroves
Landsat
Change detection
Canopy cover

ABSTRACT

Mangroves globally provide a diverse array of ecosystem services but these are impacted upon by both natural and anthropogenic drivers of change. In Australia, mangroves are protected by law and hence the natural drivers predominate. To determine annual national level changes in mangroves between 1987 and 2016, their extent (by canopy cover type) and dynamics were quantified using dense time-series (nominally every 16 days cloud permitting) of 25 m spatial resolution Landsat sensor data available within Digital Earth Australia (DEA). The potential area that mangroves occupied over this period was established as the union of mangrove maps generated for 1996, 2007–2010 and 2015/16 through the Global Mangrove Watch (GMW). Within this area, the green vegetation fractional cover (GVpc) was retrieved from each available cloud-masked Landsat scene through linear spectral unmixing. The 10th percentile (GVpc10) was then determined for each calendar year by comparing these data in a time-series. The percentage Planimetric Canopy Cover (PCC%) for each Landsat pixel was then estimated using a relationship between GVpc10 and LiDAR-derived PCC% (< 1 m resolution and based on acquisitions from all states supporting mangroves, excluding Victoria). The resulting annual maps of mangrove extent and cover for Australia are the first to be generated at a continental scale and on an annual basis. These indicated that the total area of mangrove forest (canopy cover > 20%; resolvable at the Landsat resolution) varied from a minima of 10,715 ± 36 km^2 (95% confidence interval) in 1992 to a maxima of 11,388 km^2 ± 38 km^2 (95% CI) in 2010, declining to 11,142 ± 57 km^2 (95% CI) in 2017. In 2010 (maximum extent), the forests were classified as closed canopy (38.8%), open canopy (49.0%) and woodland mangrove (12.2%). The majority of change occurred along the northern Australian coastline and was concentrated in the major gulfs and sounds. The 30 national maps of annual mangrove extent represent a reference dataset, which is publicly available through the Terrestrial Environment Research Network (TERN) landscapes portal. Future efforts are focusing on the routine production of annual mangrove maps beyond 2019 as part of Australia's efforts to monitor the coastal environment.

1. Introduction

Mangroves are a major component of many tropical, subtropical and also temperate regions (Spalding et al., 1997) and occupy a variety of settings, including estuaries, inlets and islands. Where they occur, mangroves play a major role in establishing and stabilizing the coastline (Alongi, 2008). This is achieved by their ability to rapidly colonize substrates, with the subsequent trapping of sediments (e.g., by roots) leading to the formation of more permanent mud/sand areas from which further colonization can take place (Furukawa et al., 1997). However, mangroves are highly dynamic in nature, being on the land/ocean interface, and their extent, state and dynamics are influenced by freshwater and tidal inundation, salinity differences and exposure to high winds and waves (Alongi, 2008).

The ability of mangroves to colonize and retain their position is increasingly being affected by human use and alteration of the coastline, particularly given substantive infrastructure developments in southeast Asia and Asia (primarily land reclamation and aquaculture; Lucas et al., 2014; Thomas et al., 2017). As a consequence, many of the ecosystem services for which mangroves are renowned (e.g., coastal protection, habitat provision for terrestrial, estuarine and marine fauna and flora, 'blue carbon' sequestration) are compromised or lost (Friess,

* Corresponding author.
E-mail address: leo.lymburner@ga.gov.au (L. Lymburner).

https://doi.org/10.1016/j.rse.2019.05.004
Received 5 April 2018; Received in revised form 19 March 2019; Accepted 5 May 2019

2016). Mangroves are also subject to natural events (e.g., tropical cyclones) and processes (including sea level fluctuation and changes in coastal geomorphology; Chaudhuri et al., 2015), which are increasingly being exacerbated by human-induced alterations of climate regimes.

In Australia, mangroves are protected by Federal and State laws, with over 19% (in area) located within areas assigned as an International Union for the Conservation of Nature (IUCN) protected area category. The vast majority of mangroves are therefore unaffected or indirectly affected by human activities (Asbridge et al., 2016). Mangroves are nevertheless vulnerable to a range of natural events and processes, including tropical storms (cyclones; Lugo, 2000), ambient conditions (e.g., temperature, rainfall), variable river discharges and sea level fluctuation (Ellison and Farnsworth, 1997; Duke et al., 2017). The impacts of such changes have not, however, been adequately quantified at national, regional or even local levels partly because of their dispersed coverage, remoteness and inaccessibility.

The majority of mangrove mapping for Australia has primarily utilized remote sensing data and has been undertaken through global projects. Most national efforts have combined maps generated at the State and Territory level (e.g., Australia's National Forest Inventory). The main global mapping efforts have focused on the classification of Landsat sensor data from 2000 and adjoining years (Giri et al., 2011) and the collation of nationally-generated datasets for the nominal years of 1960–1996 and 1999–2003 (Spalding et al., 1997 and Spalding et al., 2010 respectively). Notable examples of regional or state-level products are a Landsat-derived map of north Australian (the majority of Queensland and the Northern Territory) mangroves by species types (either dominant or mixed; Hay et al., 2005) and the Queensland Herbarium Regional Ecosystem (RE) maps, which include mangroves (Neldner et al., 2017). Australia's State of the Forest Report (SOFR, 2013) provides national estimates of mangrove extent by tenure, with this information collated from State and Territory sources. The estimated extent of mangroves reported in the State of the Forest Report (SOFR, 2013) in 2011 was 9130 km^2. Although some temporal and update mapping has been undertaken, the majority are for single years and hence are often static products. The Global Mangrove Watch (Lucas et al., 2014; Thomas et al., 2017; Bunting et al., 2018), supported by Japan's Aerospace Exploration Agency (JAXA) Kyoto and Carbon (K&C) Initiative, has been the first global initiative to map the changing extent of mangroves; in 1996, annually between 2007 and 2010, and 2015 and 2016.

For over 30 years, the Landsat Thematic Mapper (TM), Enhanced TM+ (ETM+) and Operational Land Imager or OLI) have provided a high temporal frequency (every 16 days, cloud permitting) moderate resolution (~30 m) time-series that continues to provide unique insights into the Earth's changing environment (Wulder et al., 2016). Until 2008, the uptake and use of these data had been relatively limited and often restricted to small areas and relatively few points in time, largely because of the cost of these data and the lack of sufficient computer storage and processing capability. However, with the public release of the Landsat archive in 2008 (Wulder et al., 2012) at no cost and developments in computing infrastructure, the use of these data for a wide range of environmental applications has increased substantially. For Australia, the entire archive of Landsat sensor data have been collated within Digital Earth Australia (DEA; Lewis et al., 2017), which aims to realise the full potential of Earth Observation (EO) data holdings by addressing the Big Data challenges of volume, velocity and variety that otherwise limit the usefulness of EO data. The foundations and core components of the DEA are a) data preparation, including geometric and radiometric corrections of EO data to produce standardized surface reflectance measurements that support time-series analysis, b) collection management systems that track the provenance of each data cube product and formalise re-processing decisions, c) the software environment that can manage and interact with the data, and d) a supporting high performance computing environment, which is provided by the Australian National Computational Infrastructure (NCI) at the Australian National University (ANU). Increasingly, the data cube approach is allowing analysts to extract rich new information from EO time series, including through new methods that draw on the full spatial and temporal coverage of existing archives. To enable easy-uptake of DEA, and facilitate future cooperative development, the code is developed under an open-source Apache License (Version 2.0), which is enabling other organisations, including the Committee on Earth Observing Satellites (CEOS), to explore the use of similar data cubes in developing countries. DEA provides capacity to integrate and apply algorithms for mapping environmental change at a continental level and since 1987, with notable successes being the Water Observations from Space (WofS) (Mueller et al., 2016) and intertidal extent modelling (Sagar et al., 2017).

Using the capacity of DEA, the aim of this research was to establish the annual dynamics of mangroves across Australia between 1987 and 2016 for the purposes of informing on environmental change impacts, including those related to climate (e.g., sea level rise and changes in storm positions, frequencies and intensities) and ultimately better inform management of mangrove ecosystems. The specific objectives were to:

a) Calculate the green fractional cover (GV) from all available cloud-free Landsat pixels for each year of observation and compare these over an annual time series to identify areas where green cover persists throughout the year.
b) Establish a relationship between the 10th percentile of green fraction (GV_{10}) observed within a year and Planimetric Canopy Cover percentage (PCC%), derived from < 1 m spatial resolution canopy masks based on LIght Detection And Ranging (LiDAR) data, with this representing a unit that relates directly to forest cover.
c) Constrain the PCC% estimates to areas known to contain mangroves, with this achieved through reference to the Global Mangrove Watch (GMW) thematic layers for 1996, 2007–10 (annually) and 2015/16.
d) Apply PCC% thresholds to map mangrove forest extent (based on a pre-determined 20 PCC% threshold) and differentiate structural categories; namely, woodland (20–50%), open forest (50–80%), and closed forest (> 80%).
e) Quantify the change in the extent of mangrove forest and canopy cover types over the period 1987 to 2016 at a national scale and establish relevance at regional (e.g., State/Territory) and local levels.

2. Study area

2.1. The Australian coastal landscape

Australia has approximately 35,500 km of coastline, large sections of which are occupied by mangroves particularly in the tropical and subtropical regions. The distribution and characteristics of mangroves is controlled primarily by climate, the geomorphology of the coastal zone and, to a certain extent, lithology and the composition and dynamics of coastal vegetation communities, including the mangroves themselves. At a national level, and on the basis of these attributes (as well as flora and fauna distributions), the landscape has been categorized through the Interim Biogeographic Regionalisation for Australia (IBRA; Department of the Environment, 2016) as these are relevant with respect to the mangrove communities and their response to environmental changes.

2.1.1. Climate influences on mangroves

The distribution, structure and diversity of Australian mangrove ecosystems is determined and influenced by climate, and particularly temperature and rainfall (Osland et al., 2017; Ward et al., 2016; Wells, 1983). The relationship between Koppen zones (Peel et al., 2007) and mangrove communities in Australia are described in Table 1.

Mangrove species diversity broadly declines with increasing latitude

Table 1
description of mangrove communities with respect to Köppen climate class in Australia.

Köppen class	Mangrove community description	Region within Australia
Am (monsoon) Aw (savannah) Cfb (warm oceanic/humid subtropical)	Extensive, productive and floristically diverse	Northern coastline, Queensland coast, northern NSW, northern WA
Cfb (temperate oceanic) Csb/Csa (Mediterranean) BSk/BSh/Bwh (semi/arid - desert)	Dispersed, lower productivity, lower species diversity	Southern NSW, Victoria, South Australia

from a maximum of 39 species in the Wet Tropics Bioregion to 1–2 in drier regions and southern range extremities (i.e., *Avicennia marina*) (Ricklefs and Latham, 1993). Rainfall in Australia is generally greater close to the coast although highly variable and, in the northern regions, occurs mainly in the summer months, largely because of the influence of monsoon systems. This frequently results in high humidity and frequent flooding. Further south, rainfall is greatest in the winter months as frontal systems are more frequent (Bureau of Meteorology, 2016). The tropical regions in the north of Australia are affected by cyclone events of varying severity (Australian Government, 2013) and also to climatic variability, which can contribute to fluctuations in sea level that can exceed several tens of centimeters in this region (Lovelock et al., 2017).

2.1.2. Geomorphologic and lithologic influences on mangroves

Along the coastline of Australia, a wide range of coastal landform (or geomorphological) types have been recognized and described on the basis of topography, elevation, shape and composition (e.g., based on rock types, unconsolidated materials; Woodroffe, 1995). The geomorphic variability is reflected in the IBRA descriptions (Department of the Environment, 2016), which include coastal plains (e.g., along the Gulf of Carpentaria) but also more topographically diverse areas (e.g., the Kimberley; Cresswell and Semeniuk, 2011). Tidal ranges are high in the north of Australia (Egbert and Erofeeva, 2010), in particular, and the extent of inundation at the higher tidal levels is greatest in low lying and flat terrain. Many mangrove areas are sheltered from high energy waves, including along the north-east tropical coastline (as these are moderated by the Great Barrier Reef), the northern coast (because of reduced exposure to large oceanic pressure systems and fetches) and southeastern Queensland (because of an extensive chain of sand islands). Along the coast of New South Wales, ocean waves impact the exposed portions of the coastline and hence mangroves are generally smaller in extent, dispersed and confined to sheltered embayments and estuaries. The varying lithologies also influence mangrove distributions as these determine (in part) the delivery of different sediment types and amounts to the coastal margin.

2.1.3. Vegetation influences

By stabilizing sediments, mangroves create an environment that is conducive to colonization (through propagule dispersal), growth and also succession by a range of vegetation species, including mangrove and non-mangrove (e.g., saltmarsh). Once established, further expansion of mangrove and other coastal vegetation occurs (Woodroffe, 1995). Different mangrove species and growth states are also subject to and respond differently to coastal influences, including cyclones, flooding and tidal surges, wave action and sea level fluctuation. Hence, the composition (in terms of structure and floristics) can change over time through the response of mangroves to the changes in the coastal environment.

3. Methods

3.1. Defining the maximum extent of mangroves within Australia

To define the limits of mangrove extent to constrain the analysis, the Australian subset of the global temporal maps of mangrove extent generated by the Global Mangrove Watch (GMW; Bunting et al., 2018), supported by Japan Aerospace Exploration Agency's (JAXA) Kyoto and Carbon (K&C) Initiative, was used. The approach adopted by the GMW was first to establish a baseline map of mangroves for 2010 at a global level through a random forests classification of both Landsat sensor spectral composite data (all spectral wavebands) and Advanced Land Observing Satellite (ALOS) Phased Arrayed L-band Synthetic Aperture Radar (SAR) data. The use of both optical and radar data benefited the random forest classification as these are sensitive to differences in the species composition, cover and also distribution of woody (branch, trunk and root) material. Changes away from and within this baseline were subsequently derived for 1996 (using Japanese Earth Resources Satellite (JERS-1) SAR), annually from 2007 to 2010 (ALOS PALSAR) and for 2015 and 2016 (ALOS-2 PALSAR-2) using a histogram thresholding approach (Thomas et al., 2018). Changes in L-band HH and/or HV backscatter data reflected losses or gains in mangrove wood volume/biomass. For Australia, the union of the mangrove extent layers was considered to be the best representation of the area where mangroves occurred at some point during the period 1996 to 2016, noting that no mapping was available prior to 1996. The GMW maps were considered to be a robust estimate of the extent of mangroves because they integrated both optical and radar sensors and the combined dataset was the best available for the period of observation as no previous temporal mapping of mangrove extent had been undertaken in Australia.

3.2. Analysing Landsat TM, ETM+ and OLI data to quantify the extent and density of mangrove canopy cover

3.2.1. Landsat sensor data

All available observations by the Landsat 5 TM, ETM and OLI from 1987 onwards were compiled and stored at the NCI and integrated within DEA. These data were available as analysis ready having been geometrically corrected, converted to surface reflectance, adjusted for solar illumination and viewing angles and masked for cloud and cloud shadow (Irish, 2000; Li et al., 2010; Zhu and Woodcock, 2012; Mueller et al., 2016; Lewis et al., 2017). The Landsat images are projected using the Australian Albers projection (ESPG:3577) with a 25 m pixel size and divided into 100 × 100 km indexed tiles, which allows individual pixel values for the same location to be accessed and interrogated.

3.2.2. Annual green vegetation fractional cover

The Landsat fractional cover was analysed using the workflow defined in Fig. 1. Within DEA, a spectral unmixing algorithm for green photosynthetic vegetation, non-photosynthetic vegetation and soil was applied to each terrain corrected Landsat surface reflectance observation (Gill et al., 2017). For each year (from 1987 to 2016), the 10th percentile of the green photosynthetic fraction (GV_{10}) was calculated, which identified vegetated areas that are persistently green throughout the year. As mangroves typically display this characteristic, they can be distinguished from grasses, wetland vegetation (e.g. reedbeds, forbs) and woodlands (e.g., savanna woodlands dominated by, for example, *Eucalpytus* or *Acacia* forests), which follow a more fluctuating and seasonal trend in greenness. Some coastal vegetation types (e.g.,

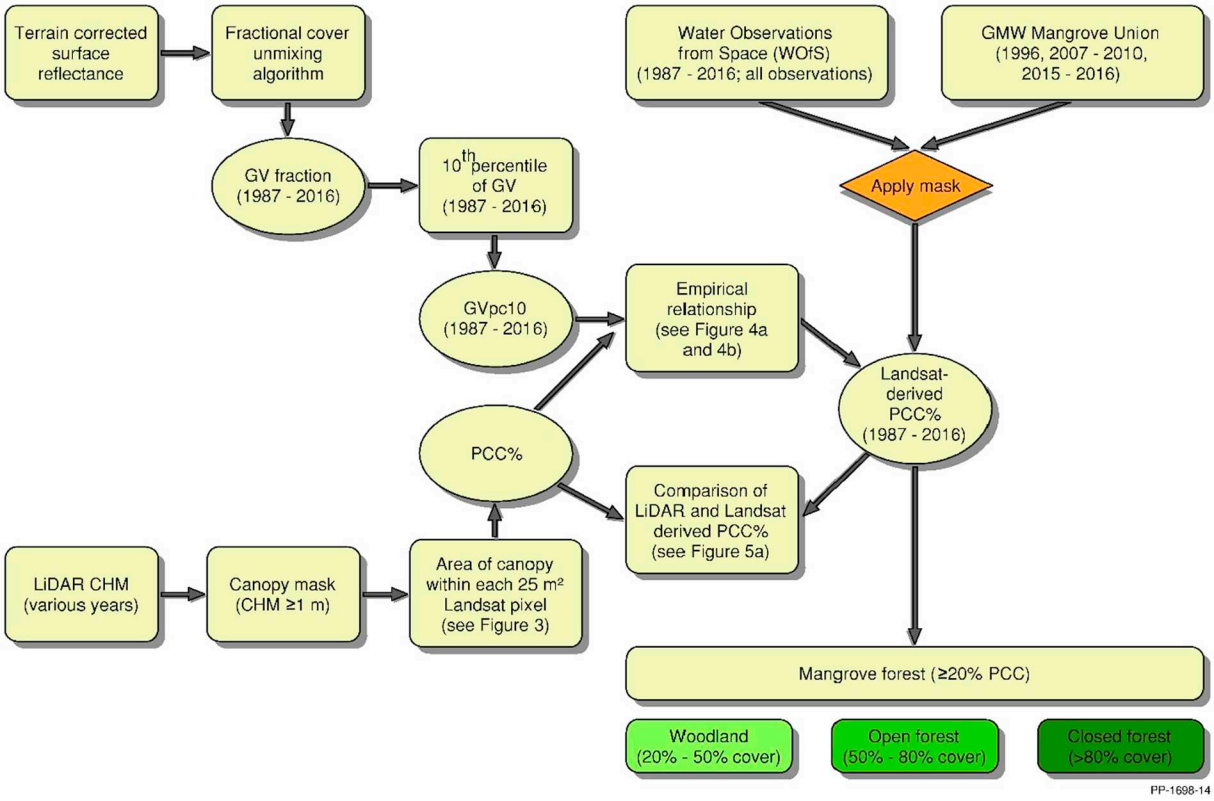

Fig. 1. Flow chart of methods used to generate annual estimates of planimetric canopy cover (%, PCC%) by forest cover type from Landsat sensor data and LiDAR-derived canopy height models.

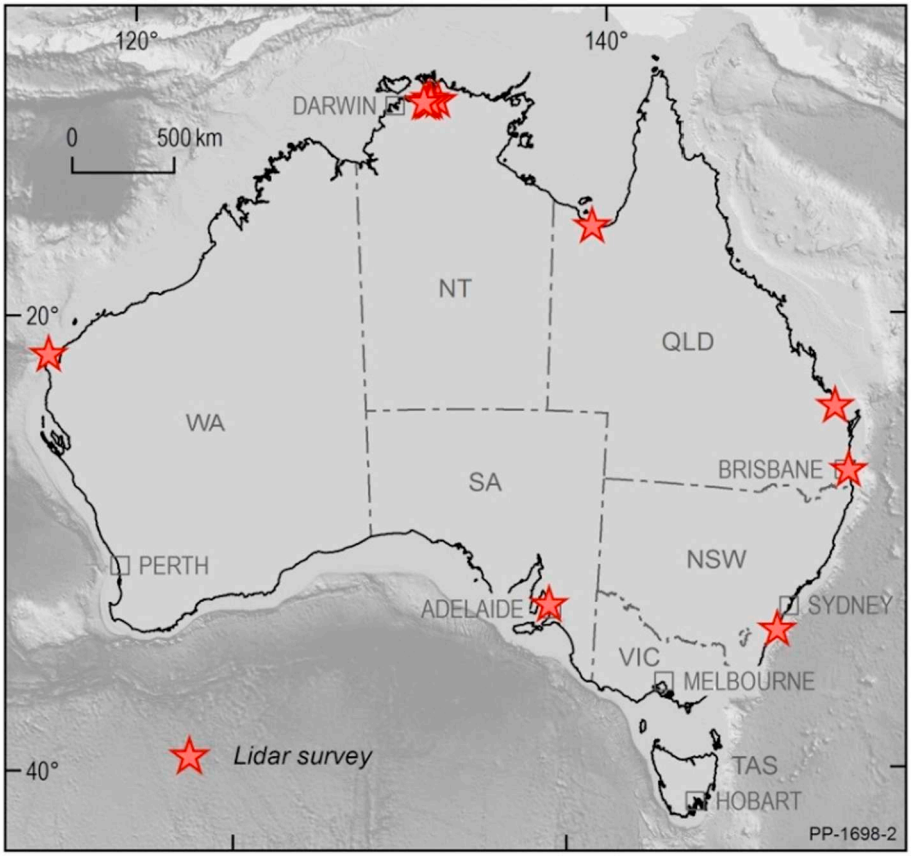

Fig. 2. The location of airborne LiDAR surveys (2006–2016) that facilitated generation of ≥1 m canopy height models (CHMs) and retrieval of PCC%.

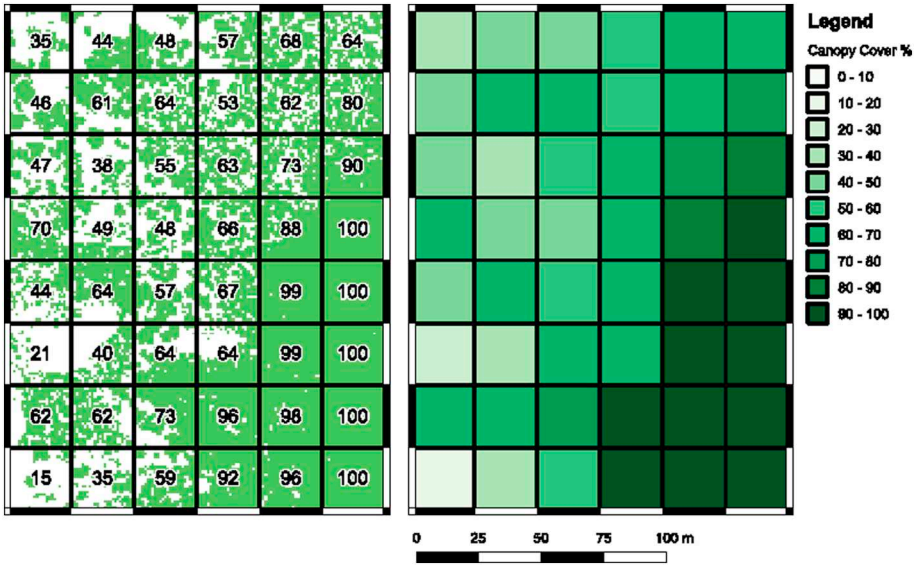

Fig. 3. Estimates of PCC% for mangroves within a section of the Leichhardt River, northern Queensland. The grid relates to the 25 m Landsat pixel resolution and the CHM (≥1 m) mask was derived from LiDAR data (based on the method of Asbridge et al., 2016).

Table 2
Accuracy assessment metrics for the series of mangrove maps.

	Area (km^2)	Area Standard Error (km^2)	agreement	agreement standard error	allocation disagreement	quantity disagreement	producer accuracy	users accuracy	omission	commission
1988	10,883	37.7	0.984	0.0049	0.0027	0.0130	0.93	0.993	0.0143	0.0013
1989	10,894	37.5	0.984	0.0049	0.0026	0.0130	0.93	0.993	0.0143	0.0013
1990	10,942	37.6	0.983	0.0050	0.0027	0.0139	0.93	0.993	0.0152	0.0013
1991	10,811	36.6	0.984	0.0049	0.0026	0.0131	0.93	0.993	0.0144	0.0013
1992	10,715	35.9	0.985	0.0048	0.0026	0.0123	0.93	0.993	0.0136	0.0013
1993	10,716	35.4	0.985	0.0048	0.0025	0.0124	0.93	0.993	0.0136	0.0013
1994	10,794	36.0	0.985	0.0048	0.0026	0.0123	0.93	0.993	0.0136	0.0013
1995	10,900	36.0	0.983	0.0049	0.0026	0.0140	0.93	0.993	0.0153	0.0013
1996	10,981	36.5	0.983	0.0049	0.0026	0.0140	0.93	0.993	0.0153	0.0013
1997	10,990	36.4	0.983	0.0050	0.0026	0.0148	0.92	0.994	0.0161	0.0013
1998	11,074	36.8	0.983	0.0050	0.0026	0.0148	0.92	0.994	0.0161	0.0013
1999	11,095	37.8	0.983	0.0049	0.0026	0.0139	0.93	0.994	0.0152	0.0013
2000	11,011	36.9	0.984	0.0049	0.0026	0.0139	0.93	0.994	0.0152	0.0013
2001	11,132	37.8	0.983	0.0050	0.0026	0.0147	0.93	0.994	0.0160	0.0013
2002	11,171	37.7	0.982	0.0051	0.0026	0.0155	0.92	0.994	0.0168	0.0013
2003	11,224	37.4	0.982	0.0051	0.0026	0.0156	0.92	0.994	0.0169	0.0013
2004	11,099	51.5	0.982	0.0056	0.0050	0.0128	0.93	0.988	0.0153	0.0025
2005	11,186	52.1	0.981	0.0057	0.0051	0.0136	0.93	0.988	0.0161	0.0025
2006	11,206	52.5	0.981	0.0057	0.0051	0.0135	0.93	0.988	0.0161	0.0026
2007	11,104	51.9	0.983	0.0055	0.0051	0.0119	0.93	0.988	0.0144	0.0025
2008	11,283	41.3	0.983	0.0053	0.0028	0.0144	0.93	0.993	0.0158	0.0014
2009	11,248	37.7	0.984	0.0049	0.0026	0.0139	0.93	0.994	0.0152	0.0013
2010	11,267	37.3	0.983	0.0049	0.0025	0.0140	0.93	0.994	0.0152	0.0013
2011	11,388	38.1	0.983	0.0050	0.0026	0.0147	0.93	0.994	0.0160	0.0013
2012	11,250	37.0	0.982	0.0050	0.0025	0.0156	0.93	0.994	0.0169	0.0013
2013	11,278	37.2	0.982	0.0050	0.0026	0.0156	0.93	0.994	0.0169	0.0013
2014	11,256	37.3	0.983	0.0050	0.0026	0.0147	0.93	0.994	0.0160	0.0013
2015	11,362	37.9	0.981	0.0051	0.0026	0.0164	0.92	0.994	0.0177	0.0013
2016	11,276	57.4	0.979	0.0063	0.0056	0.0158	0.92	0.986	0.0186	0.0028
2017	11,142	56.7	0.980	0.0062	0.0056	0.0140	0.92	0.986	0.0168	0.0028

tropical rainforests, freshwater inundated wetlands) do however have a similar level of persistence in green cover throughout the year. Mangroves were however distinct from these vegetation types within the Landsat visible, near infrared and shortwave infrared wavebands which had been integrated in the GMW random forest classification of global (including Australia) mangrove extent. The GMW maps (see Section 3.3) therefore allowed confusion with terrestrial vegetation types to be minimized.

3.2.3. *Annual water extent masks*

DEA's Water Observations from Space (WOfS) product (Mueller et al., 2016), generated from the same Landsat sensor data, provided a binary mask of water presence/absence for each Landsat scene available within the archive. These masks were summarised to generate an annual water masks based on those pixels observed as inundated > 50% of the time, which was used to identify and remove GV_{10} pixels associated with open water.

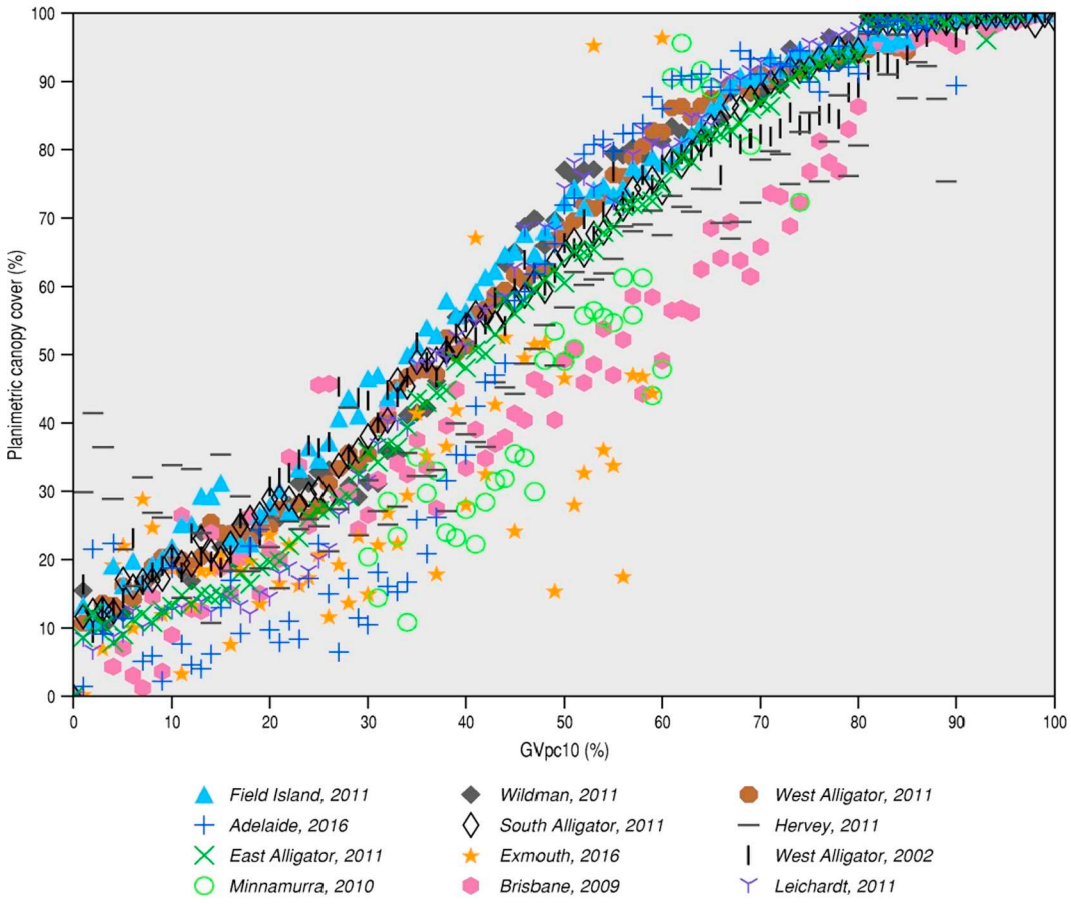

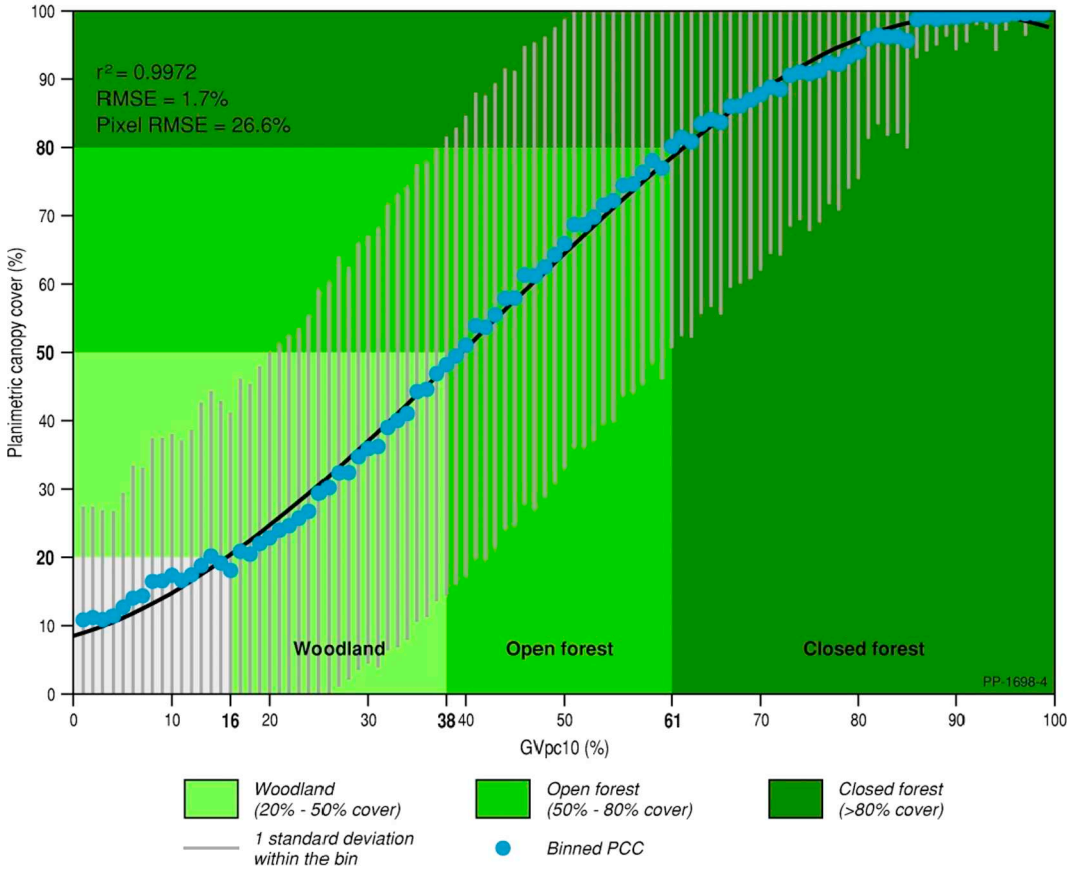

(caption on next page)

Fig. 4. Correspondence between GV10 and PCC% for a) sites in the NT, QLD, NSW, SA, NSW and WA and b) all sites combined, with PCC% binned relative to the y axis to differentiate woodland, open fore and closed forest,

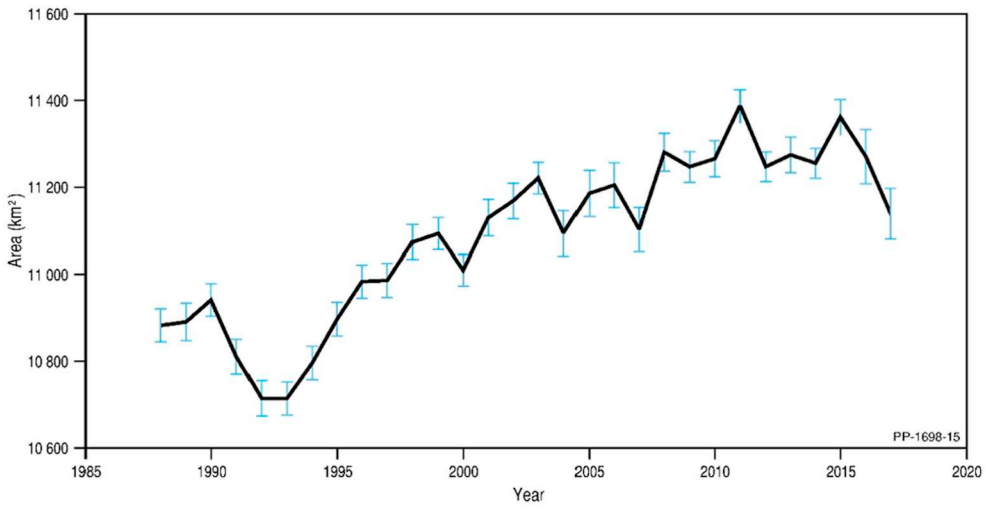

Fig. 5. Area of mangroves (km2) in Australia between 1987 and 2017. The pale blue whiskers indicate the 95% confidence interval. (For interpretation of the references to colour in this figure legend, the reader is referred to the web version of this article.)

3.3. Linking the 10th percentile of green vegetation cover fraction (GV_{10}) to Planimetric Canopy Cover (PCC%)

Forest canopy cover is defined as the proportion of the forest floor covered by the vertical projection of the tree crowns (Korhonen et al., 2006) and is a key biophysical measure. Of note is that the United Nations (UN) Food and Agriculture Organisation (FAO) defines forests as areas of vegetated land with actual/potential canopy covers and height exceeding 10% and 5 m respectively. Many countries also use this same definition of canopy cover to define their forest estate and further differentiate classes within the mapped areas (Romijn et al., 2013).

A number of standardized approaches to describing and quantifying the canopy cover of woody (woodland and forest) vegetation have been established, with these typically measuring the vertical projection of foliage (e.g., Foliage Projective Cover; FPC), all plant material (Plant Projective Cover; PPC) or the perimeters of canopies (Fiala et al., 2006). The latter either considers gaps (referred to as 'traditional canopy cover') or the canopy to be effectively opaque (termed 'effective canopy cover'). Planimetric Canopy Cover Percent (PCC%), in this study, is equivalent to the traditional canopy cover measure and is summed over a unit area (in this case, a 25 m grid cell). PCC% can also be retrieved from LiDAR data, which can detect gaps in the canopy.

To establish the link between GV_{10} and PCC%, delineation of the mangrove forests was undertaken from $\sim \leq 1$ m resolution canopy height models (CHMs) derived from Light Detection And Ranging (LiDAR) data acquired over sites in South Australia, New South Wales, Queensland, the Northern Territory and Western Australia (Fig. 2). These maps can be downloaded from Australia's Terrestrial Environmental Research Network (TERN) Data Discovery Portal (https://portal.tern.org.au). Whilst a range of higher resolution datasets exist, those derived through segmentation or using relatively coarse (> 1 m) resolution data were insufficient to resolve the required level of detail in crown cover. As examples, the mangrove extent maps for Kakadu National Park in Australia's Northern Territory obtained through segmentation of aerial photography (Asbridge and Lucas, 2016) or from 5 m resolution RapidEye data (Lucas et al., 2017) did not sufficiently resolve gaps in the canopy and hence PCC% was overestimated. For this reason, only extent maps generated through pixel-level classification of airborne LIDAR (Asbridge and Lucas, 2016) were used. The PCC% estimates derived from these data were then intersected with the Landsat pixel grid defined by DEA on which the GV_{10} was projected (Fig. 3). Within each Landsat pixel, a count of the CHM pixels was made which was divided by 625 (i.e., the number of 1 m pixels contained within each 25 m pixel) providing a measure of the PCC% for each Landsat resolution (~25 m) pixel. The resulting dataset consisted of 280,814 25 m pixel estimates of PCC% that could be linked to GV_{10}. All LiDAR CHMs used in this study had a spatial resolution of 1 m to ensure that the gaps in the canopy were resolved in a consistent way. Of these, 50% were used to establish the relationship between GV_{10} and PCC%, following grouping into 1% bins whilst the remaining 50. % were reserved for validating the resulting mapping. Binning was undertaken to reduce noise, as shown by Asbridge and Lucas (2016), which arises partly from misalignments of the airborne data and the Landsat pixel grid of the derived canopy cover products.

Australia's State of the Forests Report (SOFR, 2013, 2018) defines forests as vegetation that occupies "An area, incorporating all living and non-living components, that is dominated by trees having usually a single stem and a mature or potentially mature stand height exceeding 2 m and with existing or potential crown cover of overstorey strata about equal to or > 20%. This includes Australia's diverse native forests and plantations, regardless of age. It is also sufficiently broad to encompass areas of trees that are sometimes described as woodlands. The SOFR (2013, 2018) also distinguishes woodland forest (20 to 50%), open forest (50%–80%) and closed forest (> 80%). These thresholds were applied to the Landsat PCC% data to provide comparable estimates of the extent of these different forest categories at a national level and annually since 1987.

3.4. Validation

To assess the accuracy of each annual map of mangrove extent, 100 random points were generated for each of 11 tiles (10 × 10 km) containing > 300 ha of mangrove, with these selected to encompass all Koppen climatic zones (a stratified random sample, stratified on climate zone and area). These points were then overlain on the mangrove maps and also Landsat surface reflectance geomedian composites (Roberts et al., 2017) for each year (Table 2). An independent analyst then reviewed the mangrove classification at each point and, through visual interpretation, deciding whether the point was allocated as 'mangrove'

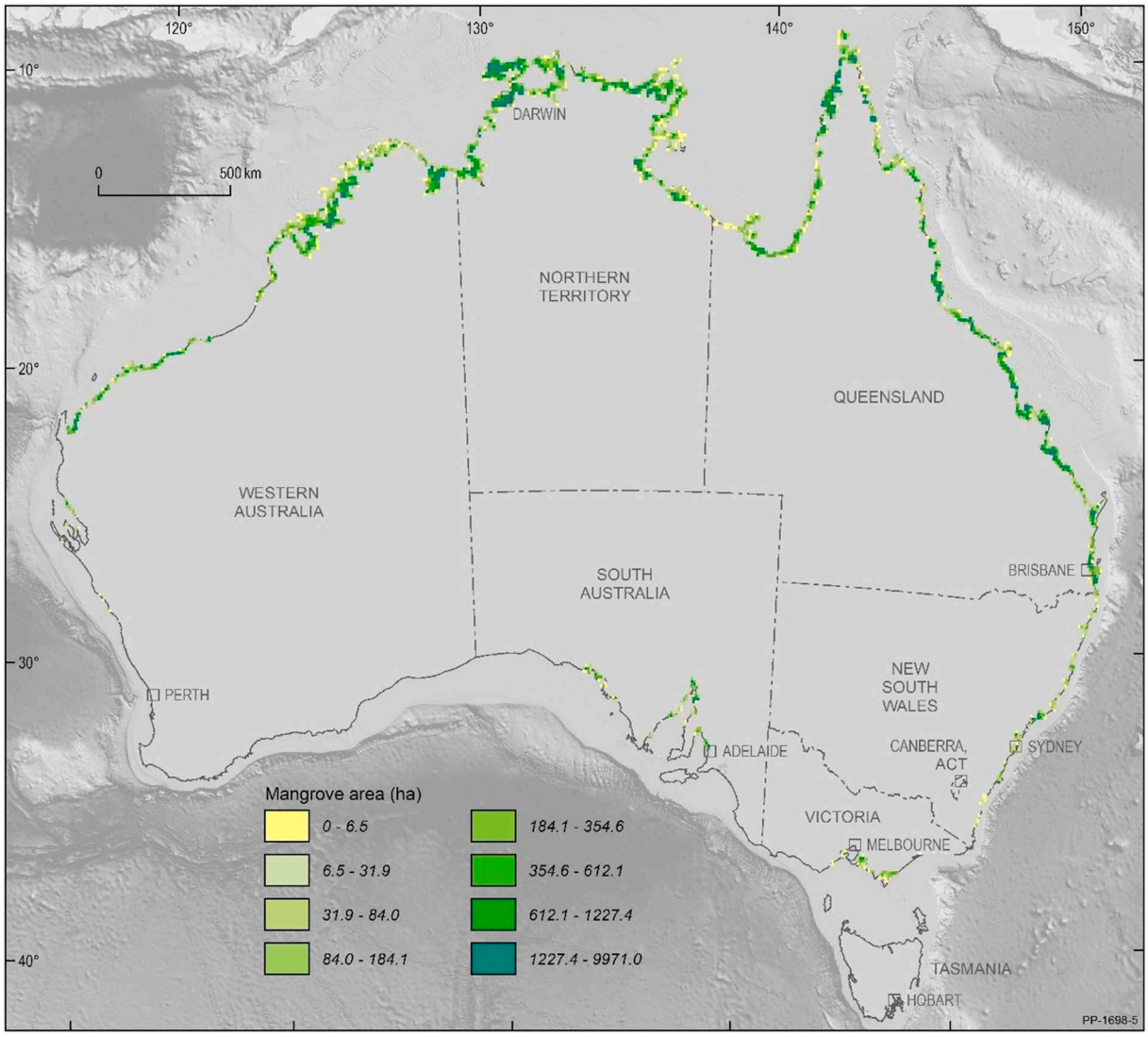

Fig. 6. The extent of mangroves in Australia in 2017. Mangrove areas is summarised on a 10 × 10 km grid to assist visualisation at the continental scale.

or 'not mangrove'. Summary statistics for the national scale product were then generated by aggregating the 33,000 points (i.e., 11 tiles × 100 points × 30 annual maps), with these being area estimation uncertainty (Olofsson et al., 2013), allocation and quantity agreement (Table 2; Pontius Jr and Millones, 2011) and users' and producers' accuracy (Table 2; Congalton, 1991).

4. Results

The following sections outline the estimation of PCC% from GV_{10} (Section 4.1), a description of the areal extent of mangroves and it's uncertainty (Section 4.2), and mangrove canopy cover and how it has changed over time (Section 4.3).

4.1. Estimation of planimetric canopy cover (PCC%) from the 10th percentile of green vegetation cover fraction (GV_{10})

Following the approach of Asbridge and Lucas (2016), a non-linear relationship was observed between the average PCC% from GV_{10} binned at 1% intervals for all LIDAR sites in NSW, Queensland, the Northern Territory and West and South Australia. The relationship was relatively consistent between sites, which represented a range of settings, and also years in which the airborne data were acquired (i.e., 2002 to 2016; Fig. 4a). The most consistent relationships were associated with the airborne LIDAR captures acquired in the Northern Territory and northern Queensland (Kakadu National Park and the Leichhardt River), with this attributed to differences in the quality of the but also the relative occurrence and proportions of mangroves and saltmarsh vegetation within the same Landsat sensor pixel, those at Minnamurra in New South Wales and Adelaide in South Australia containing greater mixes of these two vegetation types. To translate GV_{10} to thresholds of average PCC% that were relevant for distinguishing forest from non-forest but also woodland, open and closed forest categories, a 3rd order polynomial regression ($r^2 = 0.997$, RMSE = 1.6%) was fitted to the two datasets using the scikit-learn library (Pedregosa et al., 2011; Fig. 4b).

4.2. Mangrove extent

4.2.1. Accuracy assessment of the extent of mangroves

For the years of observation, the users and producers' accuracies range were 92.0–93.0 and 0.97–0.99% respectively, with the latter being consistently lower (by ~5%; i.e., for areas of mangrove in the reference dataset identified as 'not mangrove' in the national map tile). The agreement was between 97.9 and 98.5% (0.58–0.63% standard error) and disagreement ranged from 0.25 to 0.51%. These error statistics are indicative only and users are encouraged to evaluate the suitability of the maps for their particular applications and areas/times

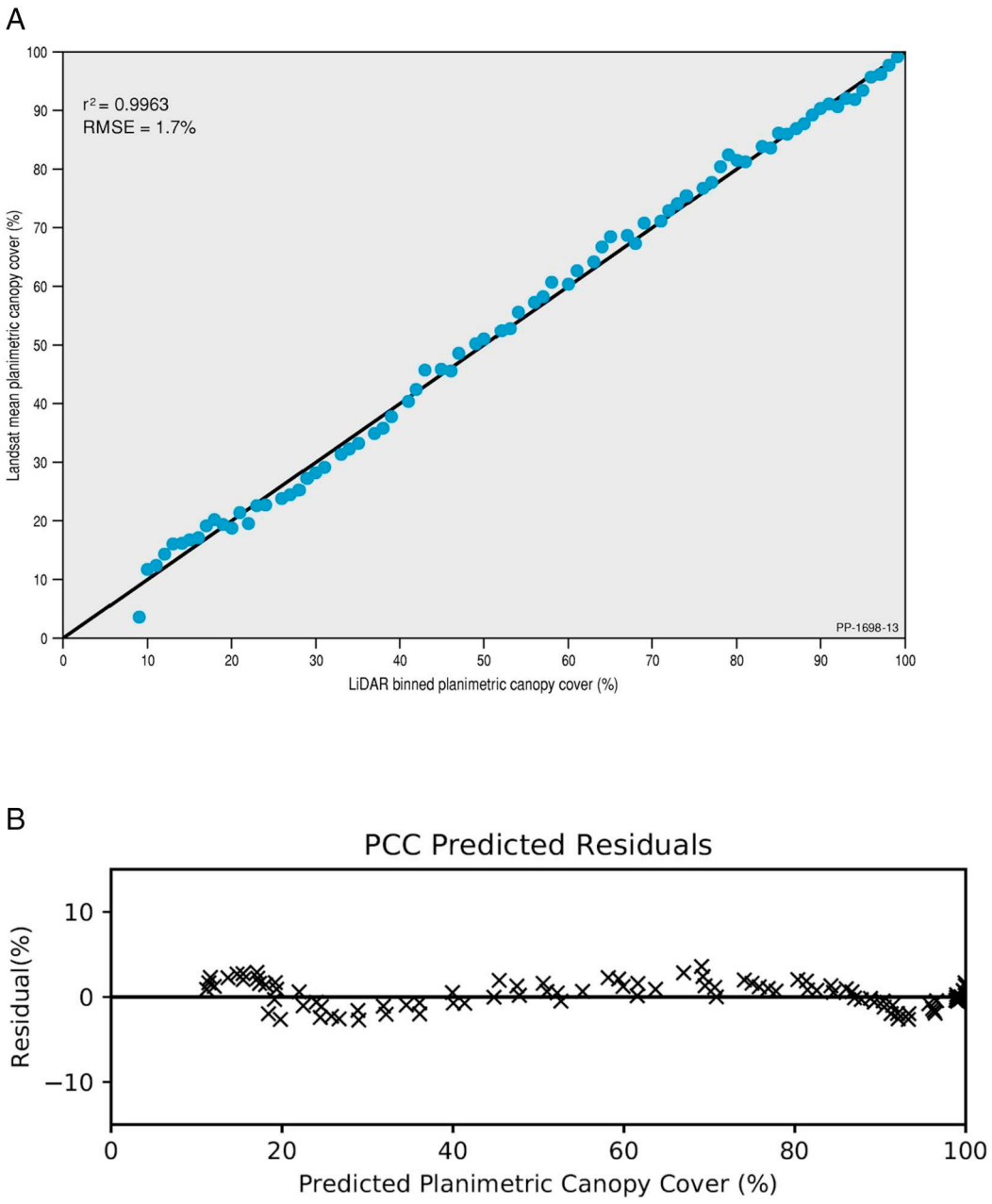

Fig. 7. a) The correspondence between Landsat estimated PCC% and an independent set of LIDAR-derived PCC%. b) Residuals between predicted and observed PCC%, with this typically being < 5% with low bias.

of interest using the following link (Mangrove_maps_on_National_Map).

4.2.2. Extent of Australia's mangroves

In 2017, the extent of mangroves across Australia, defined using a PCC% threshold of ≥20%, was 11,142 ± 57 km^2 (Figs. 5 and 6). The majority of mangrove communities occupy a range of settings (estuaries, coastal margins, inlets) along the northern and eastern coastlines. During the previous decades both the overall extent, and extent of individual classes varies as follows. Mangrove extent reached a minima of 10,715 ± 36 km^2 (95% CI) in 1992, followed by a period of expansion which reached a maxima of 11,388 km^2 ± 38 km^2 (95% CI) in 2011, this was followed by a period of decline to 11,142 ± 57 km^2 (95% CI) in 2017 (Fig. 5).

4.3. Mangrove canopy cover

4.3.1. Accuracy assessment of the canopy cover estimates

The Landsat PCC% estimates that formed the basis of the mangrove maps were validated using an independent set (50% or 140,407 points) from the LIDAR survey. A very strong correspondence between predicted (Landsat PCC%) and observed (LIDAR PCC%) binned measurements) was obtained (Fig. 7a; r^2 = 0.9963) and the Root Mean Square Errors (RMSE) for binned and pixel level data were 1.7% and 26.6% respectively. The high pixel-level RMSE was attributed to slight misalignment of the Landsat pixel grid (as per Fig. 3) with the LIDAR data, which lead to differences in the LIDAR PCC% value for a given Landsat pixel. The relationship between predicted and observed PCC% values has a very low bias of 0.083% (Fig. 7b).

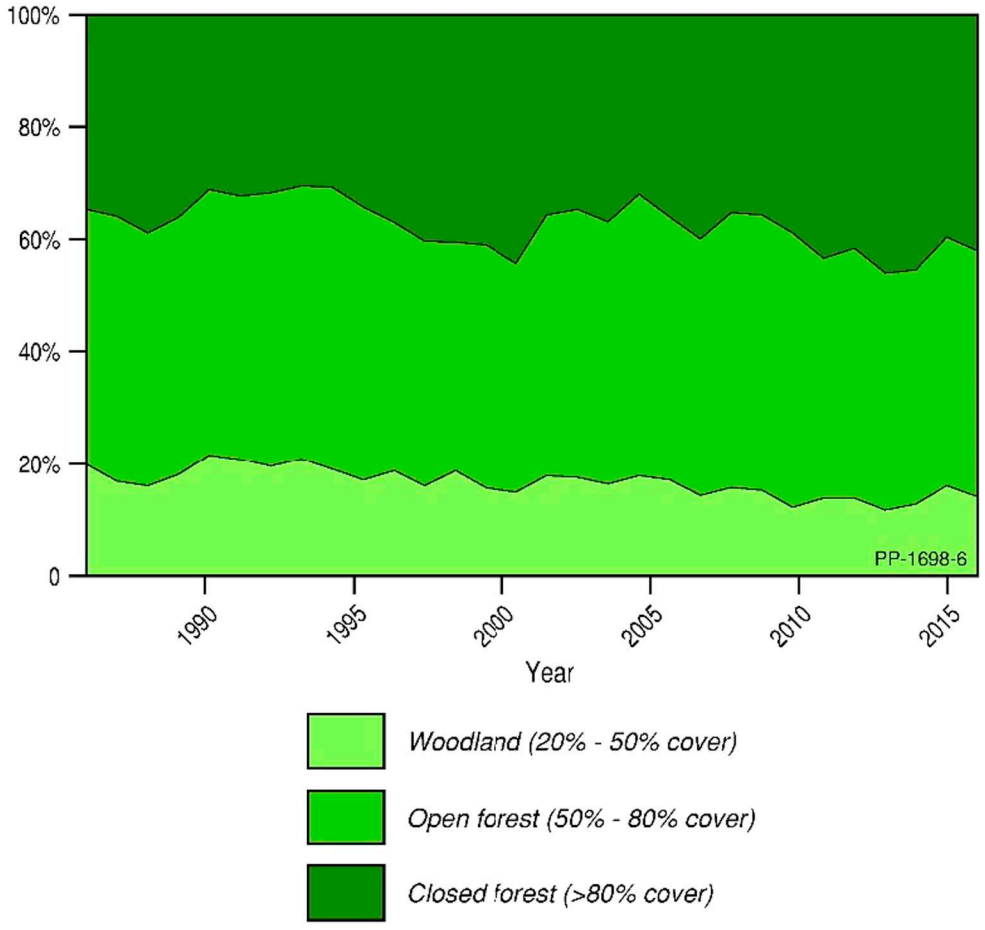

Fig. 8. Temporal trends in mangrove extent by cover class in Australia between 1987 and 2016.

4.3.2. National scale mangrove canopy cover

Fig. 8 shows the temporal changes in canopy cover at a national scale over the past three decades. Open forest (canopy cover between 50% and 80%) is the dominant class overall, with closed forest (canopy cover > 80%) second and woodland (canopy cover between 20% and 50%) third. The proportion of the woodland class is reasonably stable, declining slightly in later decades. The relationship between open and closed forest is largely reciprocal, with losses in one resulting in gains in the other. Viewing the changes in canopy cover in combination with the changes in extent at a regional scale provides some more insightful results.

4.4. Changes in mangrove area and canopy cover

4.4.1. Changes in mangrove area and canopy cover with respect to bioclimatic regions

The changes in area and canopy cover are grouped into bioclimatic regions according to the Interim Biogeographic Regionalization of Australia in Fig. 8. The 95% confidence intervals with respect to area uncertainty are not shown in Fig. 8. However, changes in area need to be greater than ~0.3% to be significant at the 95% confidence interval. Some regions, such as the Northern and Southern Great Barrier Reef (GBR), show very little variation over time, whereas others (e.g., the Dampier Coast, Bonaparte Gulf and Gulf Coast) show large amounts of change. All three regions experience a low in the early 1990s and a maxima around 2010/11.

4.4.2. Changes in mangrove area and canopy cover with during periods of expansion and contraction across northern Australia

During the period of expansion (1992 through 2010; Fig. 9a), gains were concentrated in the major gulf regions across Australia's tropical north but these same areas also experienced the greater loss in extent in the years following (2011 through 2017; Fig. 10). These losses were largely associated with the mass dieback event, causes of which included a rapid drop in sea level (Duke et al., 2017; Fig. 9b). This suggested that many of the mangrove areas experiencing dieback in 2015/16 (e.g., as reported by Duke et al., 2017 for the Gulf of Carpentaria and Lucas et al., 2017 for Kakadu National Park) were relatively recent colonists of the coastline. Furthermore, the Landsat time-series provides evidence that the extent of mangroves in the Gulf of Carpentaria started to decline as early as 2014 (Fig. 8). Of note is that, despite the dieback event, the overall area of mangroves was greater (by an estimated 427 km^2 at the national level) in 2016 compared to the minimum in 1992.

4.4.3. Changes in mangrove area and canopy cover at a local scale

The 25 m resolution of the Landsat series of sensors makes it possible to resolve where the mangrove expansion and contraction was occurring within specific estuaries (Figs. 11 and 12). As an example, mangroves within the Roper River estuary in the western Gulf of Carpentaria (Northern Territory) and the coast-facing margin experienced a period of expansion in both a seaward and landward direction between 1987 and 2010 and an increase in canopy cover (Fig. 11). However, between 2010 and 2016, the mangrove canopy cover reduced or was lost through mass tree mortality (Duke et al., 2017). These areas of expansion and contraction are highlighted in Fig. 12, which also shows similar mapping for King Sound (mouth of the Fitzroy River, Western Australia) and the Gulf of Carpentaria (mouth of the Norman River, Queensland). In the latter case, a near complete dieback of mangroves occurred along the coastline north of the Norman River

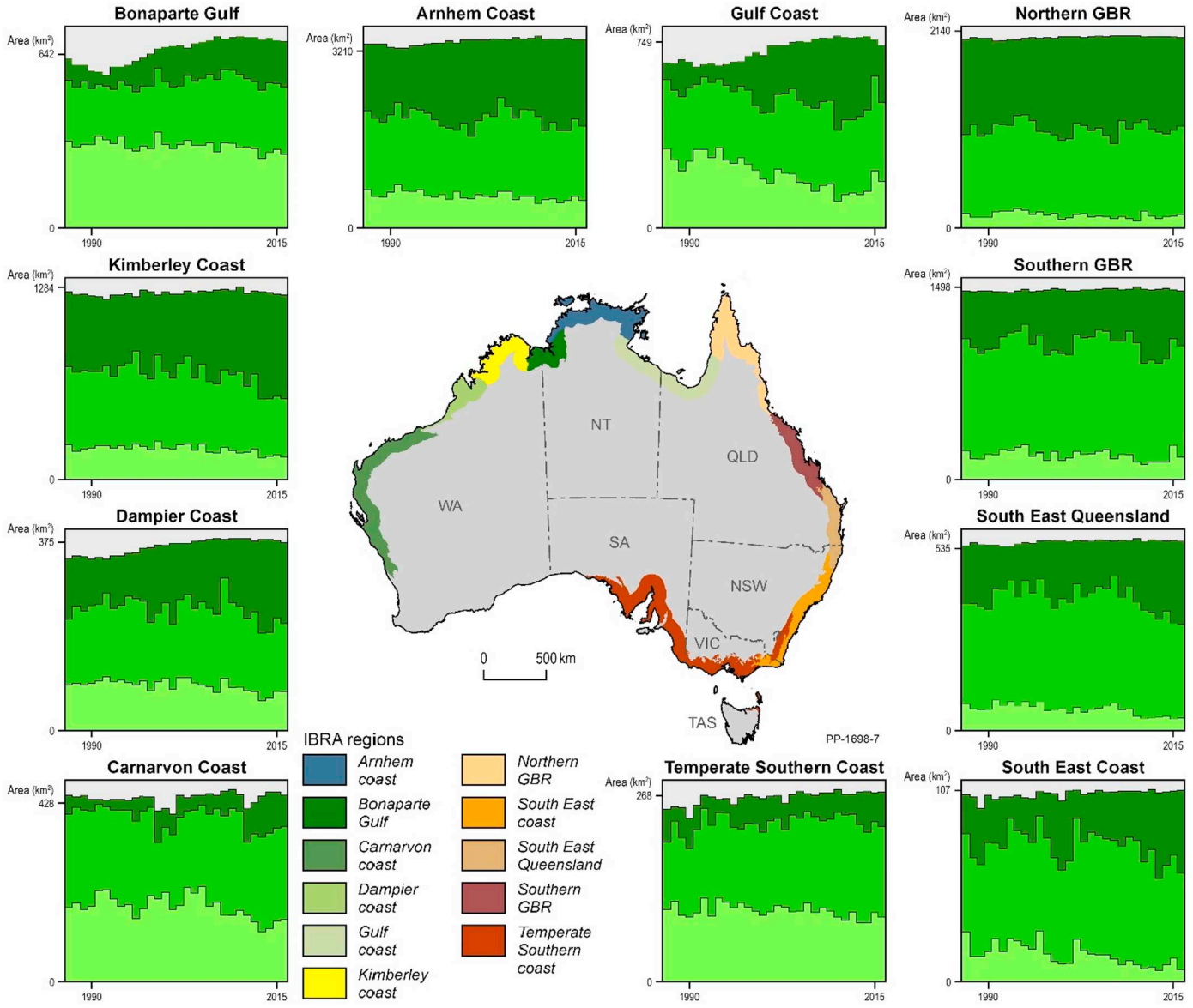

Fig. 9. Regional variations in the area of mangrove by canopy cover class.

estuary mouth. The changes are also reflected in the column charts, which highlight changes in both extent and canopy cover over the observation period.

The Roper River estuary, King Sound and the Gulf of Carpentaria are examples of locations where major fluctuations in mangrove extent have occurred (Fig. 12). A detailed representation of expansion and contraction is evident in the Roper River estuary, with the period 1987–2010 showing a noticeable increase in the area of mangroves (in both the landward and seaward directions along the coast but also on meander bends) and also canopy cover. However, the mangroves and density (all cover classes) at this location then decreases between 2010 and 2016, with this being most notable along the seaward facing shoreline. A similar overall pattern of large area expansion and increases in canopy cover followed by a period of contraction was also evident in Kings Sound. Within the Gulf of Carpentaria, a similar period of expansion was observed but the decline/loss of mangroves along the shoreline was much more prominent, leading to a sharp drop in extent in 2015/16.

4.4.4. Change in response to a severe tropical cyclone

One of the few areas in Australia's north to undergo a decline in mangroves between 1994 and 2010 was Junction Bay in the Northern Territory, with this attributed to extensive damage caused by Cyclone Monica in April 2006. This Category 5 storm made landfall west of Maningrida in West Arnhem, Northern Territory. The mangroves were heavily impacted by the severe winds and associated storm surge associated (Staben and Evans, 2008) and resulted in a loss of extent and reduction in canopy density (Fig. 13). These losses were quantified for an area 5 km either side of the recorded cyclone track and most noticeable was the rapidity in the decline of mangrove extent and the loss of all closed forest and the majority of open forest following the cyclone. The post cyclone recovery was also evidenced by an initial increase in canopy cover associated with woodlands followed by a progressive increase in open and then closed mangroves with the area of mangroves becoming similar to that noted during the immediate pre-cyclone period. However, changes in the location of some mangroves were evident and some areas where mangroves remained in place were still recovering in 2016. A decrease in closed forest and an increase in woodland forest extent were observed in 2003, which reflected mangrove recovery from a Category 3 storm.

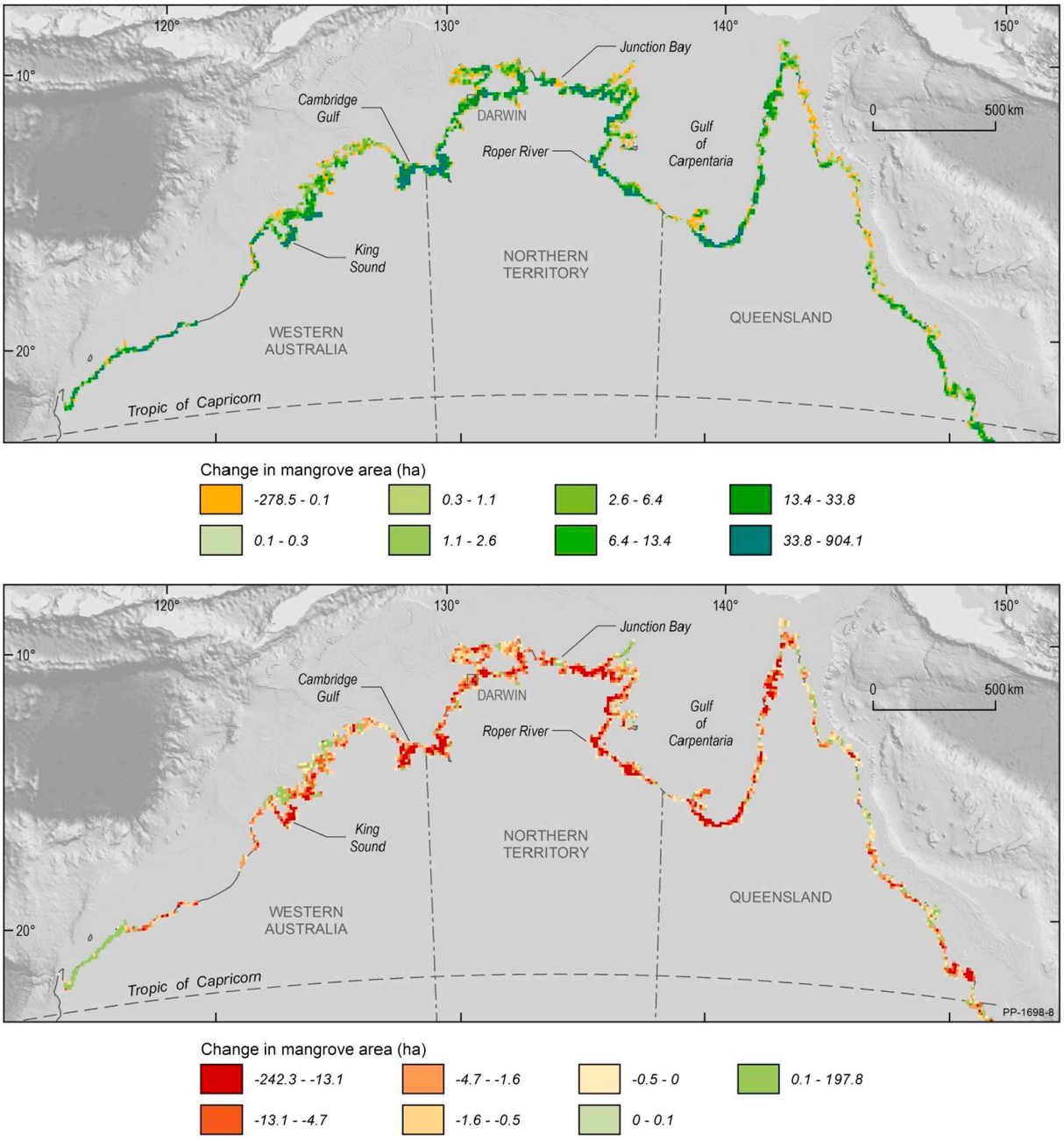

Fig. 10. a) Expansion of mangroves between 1994 and 2010 and b) decreases in mangrove extent between 2010 and 2016, with change in area shown for 10 × 10 km grid cells.

5. Discussion

5.1. The use of the 10th percentile of green vegetation cover fraction (GV_{10}) to estimate Planimetric Canopy Cover (PCC%)

The GV allowed consistent mapping of mangroves across their range as the leaves of most mangrove species are evergreen and leaf longevity (of evergreen species) typically ranges from 5 to 29 months (Saenger and West, 2016). The canopies of mangroves are typically homogeneous (e.g., in cover and height) and often occur as contiguous zones, with this contrasting with many woodland environments with which they border. Other measures, such as the Normalised Difference Vegetation Index (NDVI) can capture these characteristics to a certain extent but are subject to the variability introduced by differences in canopy openness and the complex seasonality associated with overstorey and understorey vegetation. The use of the GV largely addresses this confusion.

The GV is determined through linear unmixing of bare soil and the green and brown fractions of vegetation and does not deliver a shade/water fraction. Hence, the use of the WOfS allows areas of open water to be identified and removed, although water located within the same pixel area as the mangroves is not disaggregated. This potentially leads to inaccuracies in the PCC% product in areas such as the seaward edge fringes (e.g., dominated by more open *Sonneratia* sp.), where water is present under the canopy for a significant portion of the tidal range. A suggested future improvement on the method is the inclusion of GV obtained only from images acquired at high or low tide (Rogers et al., 2017), although this would significantly reduce the number of scenes available for retrieving canopy cover.

The method developed in this paper established a relationship

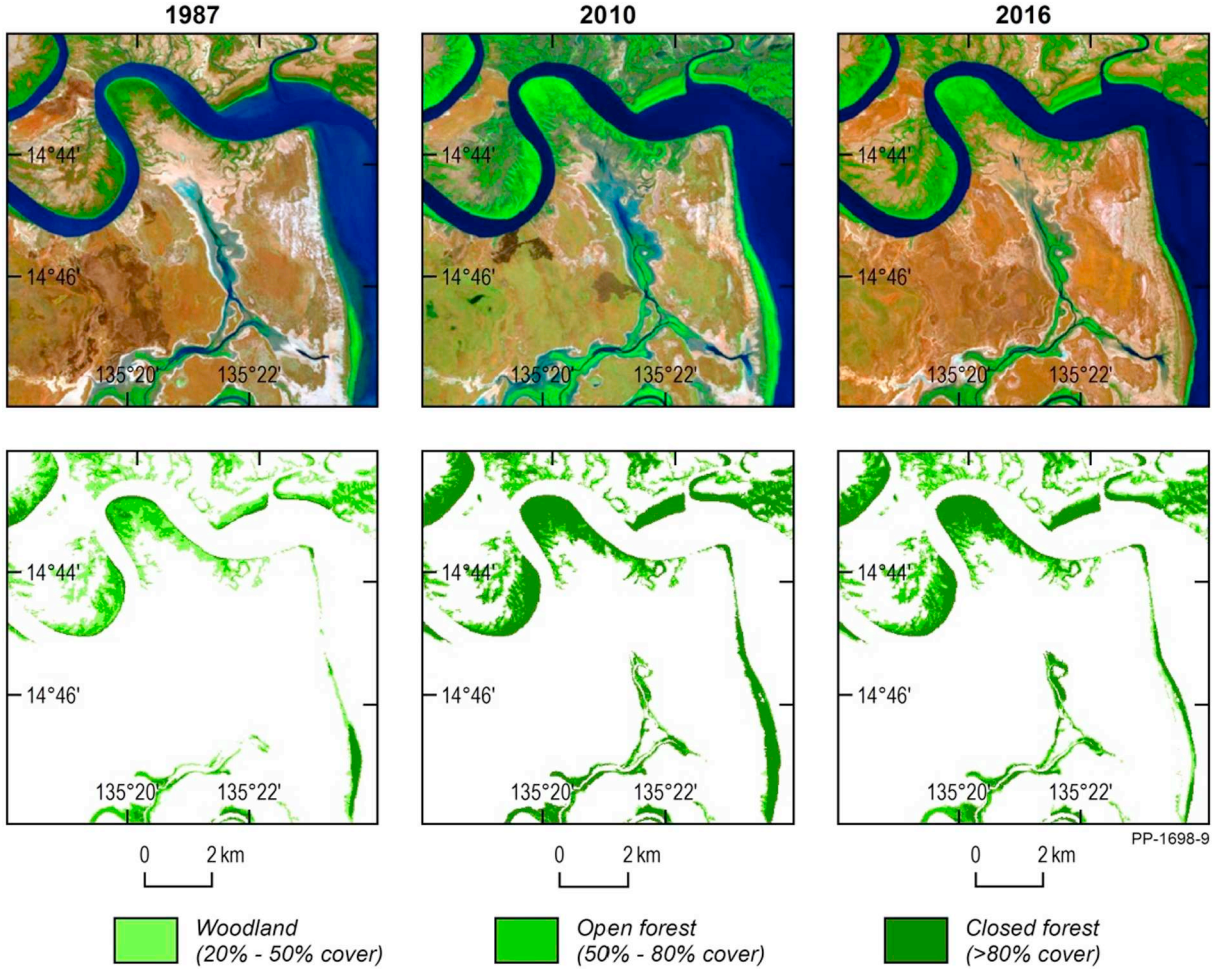

Fig. 11. Changes in the Roper River estuary and surrounding coast. The first row shows false colour imagery (October) in the years of interest as visual reference, whilst the second highlights the extent of each mangrove class (woodland, open forest, closed forest) for each reference year. Of note is the major increase in canopy cover and landward expansion between 1987 and 2010.

between GV_{10} and PCC%, as measured by $\sim \leq 1$ m resolution airborne (primarily LiDAR) data. The conversion from a statistical summary of multiple EO observations into a unit that is a recognized measurement of canopy structure makes the resulting canopy density maps easier to analyse and interpret by other domain specialists, including natural resource managers, carbon modelers and mangrove ecologists. The conversion to a measure of canopy cover also provided the basis for distinguishing mangrove forest from non-forest categories and also different forest structural categories (i.e., woodland, open and closed). When determining PCC%, only $\sim \leq 1$ m CHMs generated from lidar data were used, as these allowed the crowns of individual and clusters of trees to be delineated. Whilst field measurements of canopy cover were considered, these were highly variable in terms of the measurement procedures and limited in spatial coverage. The use of LiDAR rather than field data to establish this relationship provided a much larger number of samples across a wide range of mangrove communities.

5.2. Approach to national mapping

The 30 national maps of mangrove extent and cover type generated through DEA have been generated using a comparable threshold of PCC% and their generation represents a major advance in quantifying and understanding the state and dynamics of Australia's mangroves. Whilst other detailed maps of mangrove extent exist, the majority have only been generated for portions of the Australian coastline over specific time periods (e.g., Hay et al., 2005, Brocklehurst and Edmeades, 1996). The only other national map is that of the National Forest Inventory (NFI), which was produced from collations of mapping undertaken by the States and Territories.

The mangrove maps generated using the DEA result in an increase in area of 1396 km^2 over the 9120 km^2 reported in Australia's State of the Forest Report (2013) for the year of 2011 (Table 3). This discrepancy is attributed to the different methods used in the classification of mangroves and in the collation of disparate datasets from Australia's States and Territories.

Despite the use of 25 m Landsat sensor data, the maps generated through DEA are still relatively coarse and omit small clusters or narrow bands of mangroves (e.g., in the upper section of creeks). However, they allow mangrove extent and canopy cover to be tracked year-on-year and provide a national but also regional to local overview of events and processes that influence their states and dynamics. Furthermore, the observations on their response to cyclones (during and following the event), changes in coastal geomorphology and sea level fluctuation concur with those undertaken in other studies (e.g., Duke et al., 2017; Lovelock et al., 2017).

Of note is that the observations place the large-scale dieback event across northern Australia in 2015/16 into a broader spatial and temporal context. In particular, mangrove dieback has been shown to largely affect mangroves that had established since 1991 and largely in response to rises in sea level. Despite the dieback event, the total area of mangroves in 2016 had increased by 372 km^2 compared to the

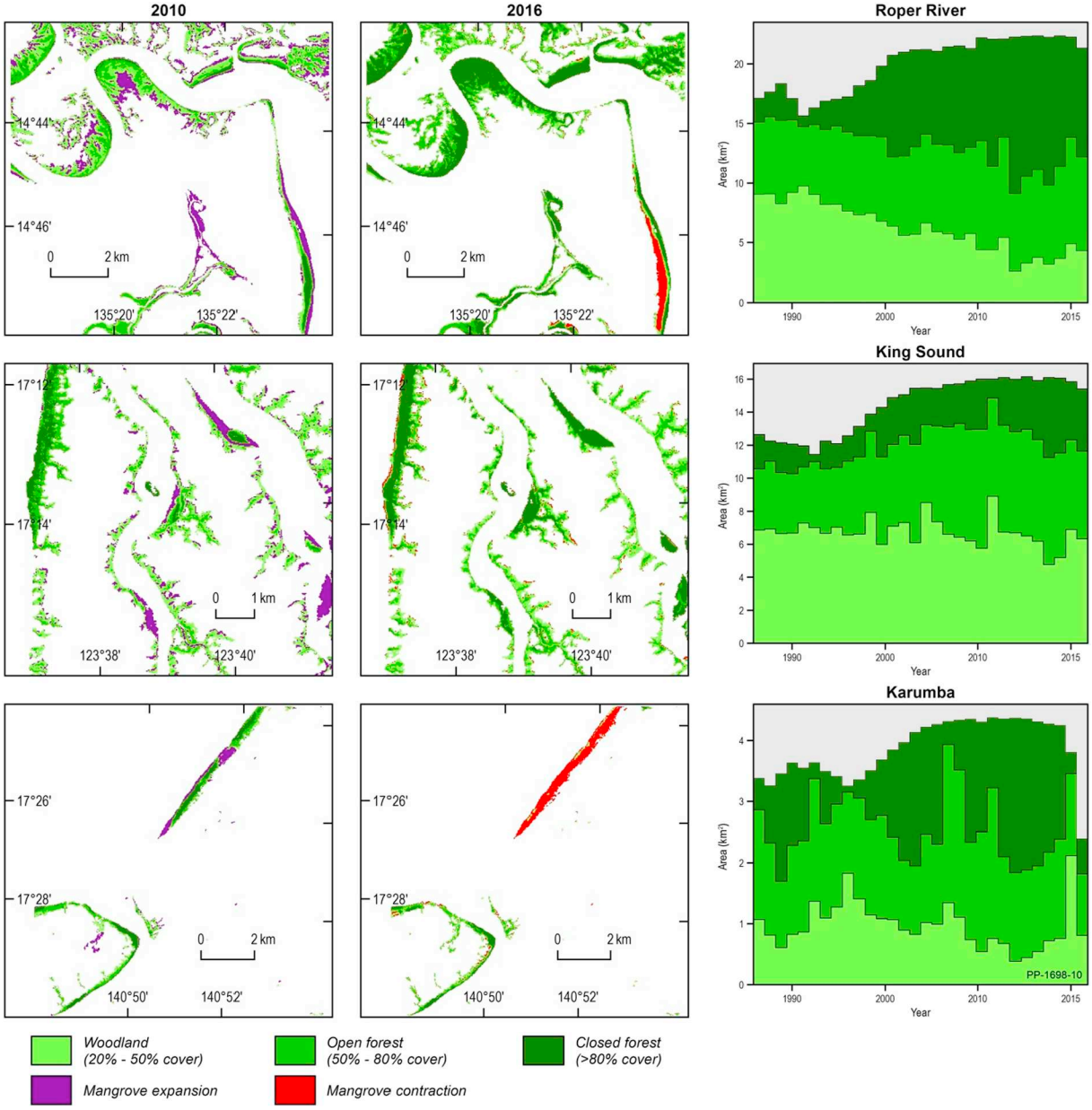

Fig. 12. Detailed patterns of the mangrove expansion that occurred between 1991 and 2010 (purple) and contraction that occurred between 2010 and 2016 (dark red) of mangrove communities in Roper River (NT), King Sound (WA), and Norman River estuary and proximal coastline (QLD). (For interpretation of the references to colour in this figure legend, the reader is referred to the web version of this article.)

minimum extent in 1992, with this change taking place partly as a result of colonization of mangroves into new areas. Dieback also occurred beyond the Gulf of Carpentaria, as reported by Duke et al., (2017), with areas affected including the Cambridge Gulf in Western Australia and the Alligator Rivers Region (Kakadu National Park; Lucas et al., 2017). Changes in mangroves along the northern coastline also disproportionately influenced the national annual figures of mangrove extent by cover type.

The dieback of mangroves is likely to be cyclical and dependent on sea level fluctuations (Asbridge and Lucas, 2016; Lovelock et al., 2017). The mangroves themselves can also migrate geographical positions over time, with this largely occurring because of changes in coastal geomorphology. However, there are areas of mangroves along the coastline which have remained in the same position and have not been adversely affected by changes in the coastal environment. These mangroves can be considered as 'core' areas, which should be recognized for their role as refugia in the event of future climatic fluctuations and hence their conservation importance (Luther and Greenberg, 2009).

5.3. Integration of global mangrove watch products

The maps of mangrove extent generated by the GMW for 1996, 2007–2010 and 2015/6 used a globally consistent algorithm, which can also be applied in subsequent years as new ALOS-2 PALSAR-2 and other L-band SAR mosaics become available. The maps generated for Australia through the DEA utilized the union of the available GMW layers to define the maximum potential extent of mangroves (based on their past distributions). In most cases, it was assumed that the GMW encompassed the area of suitable habitat for mangroves, particularly as 2010 was a year of maximum mangrove extent. However, the mapping was not available in the pre-1996 epoch and areas where mangroves occupied during this period might have been excluded. The union mask was not able to capture some mangroves which were in the upper reaches of tidal creeks and also those that were too small to be resolved

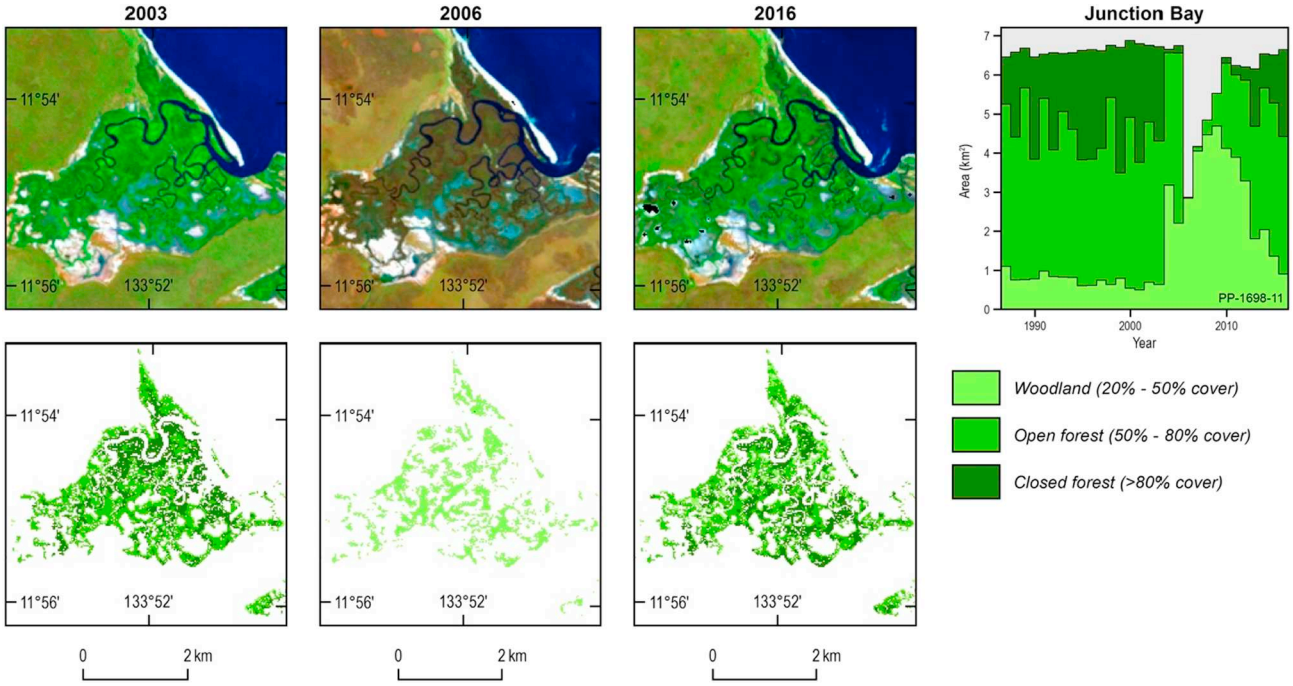

Fig. 13. Junction Bay, Northern Territory, where mangroves experienced losses in extent and cover in 2003 and 2006 as a result of category 3 (severe tropical cyclone Debbie) and 5 (severe tropical cyclone Monica) tropical storms respectively. Note that the 2003 image is prior to the impact of Debbie. The column chart indicates the extent and cover during the pre- and post-cyclone periods.

Table 3
The area (km^2) of mangroves by cover density for 2013 based on the SOFR and DEA.

Product	Total area of mangroves	Proportion of woodland	Proportion of open forest	Proportion of closed forest
SOFR	9120	(12%)	(41%)	(47%)
DEA	11,277 ± 37	(14%)	(43%)	(43%)

at the spatial resolution of observation of the Landsat sensors and ALOS sensors. As a consequence, the extent of landward expansion of mangroves, especially expansion that occurs along narrow tidal creeks, will have been underestimated.

Within the union of the GMW mangrove maps, the PCC% allowed a region-specific refinement of the mapping for these years but also all other years from 1987 onwards. The greater temporal frequency and range of observations provides a more comprehensive overview of changes in mangrove extent as well as cover. For other regions, the same or even a different approach to mapping mangroves could be applied. However, the GV product is particularly robust for Australia because of the greater amount of cloud-free pixels. Furthermore, over much of the continent, many mangroves are distinct from proximal land covers (e.g., tropical savannas, mud or sand flats) in both the SAR and Landsat sensor data, which improves their delineation. The GVpc calculation may, however, be compromised in countries where there is a greater frequency of cloud cover or where the land covers bounding mangroves are less distinct (Lucas et al., 2014).

5.4. Further work

An increase in the quality of the mangrove baseline classification is a key step which would improve the derived products and overcome the errors of omission observed in the current product. Therefore, the application of Sentinel-2, either singularly or in combination with Sentinel-1, should be investigated for producing a new 10 m resolution mangrove baseline for Australia. The availability of Sentinel 1 and Sentinel 2 data will enable the development of more spatially detailed mangrove extent and canopy density layers. This should increase insight into mangrove dynamics along narrow tidal creeks that are below the detection capabilities of the current PCC% product. Additionally, rather than simple thresholding, a classification of the Landsat imagery within the DEA could be undertaken include areas of mangroves that were present prior to the 1996 baseline to be identified.

Further work will focus on using the observed changes in mangrove extent and canopy density in combination with additional datasets to quantify the impacts of processes (e.g., sea level fluctuations) and events (e.g., severe tropical cyclones) on mangroves. The PCC% product described here have potential to be linked to in-situ measurements of allometry and soil carbon to provide insight into the dynamics of the 'blue carbon' within Australia's mangroves. This would thereby provide insight into how carbon stocks have changed in response to past disturbances. Mangrove canopies identified by the PCC% approach could potentially be classified into dominant species or zones using the methods described in Nardin et al. (2016) or Rogers et al. (2017).

The approach outlined in this paper could be applied in other regions using the Open Data Cube code base https://www.opendatacube.org. In countries where the fractional cover data are unavailable, this approach could be modified to use a percentile of annual NDVI values. However, additional analysis would be required to establish the relationship between NDVI and PCC%.

Finally, the map of mangrove extent generated for Australia through DEA are being used as a refinement of the global mangrove maps generated through the combination of Landsat sensor and Japanese L-band SAR as part of the GMW. For many countries and regions, such an approach is expected to lead to improvements in mangrove mapping and the development of measures, such as GV, within open data cube environments is advocated.

6. Conclusions

This is the first time that maps of mangrove canopy cover, at 25 m spatial resolution and using an annual time step, have been produced at a continental scale for Australia. The annual maps of mangrove canopy

cover clearly show changes in the extent and density of Australia's mangroves over the last three decades that reflect the influence of the different drivers that operate at these scales.

The area of mangroves in Australia increased between 1994 and 2010, followed by a period of contraction between 2011 and 2016. These fluctuations were concentrated around the mangrove communities in the gulfs and sounds of tropical northern Australia, whereas the mangroves on the eastern and southern coasts remained comparatively stable. Even so, severe tropical cyclones led to a considerable loss but also redistribution of mangroves by cover class although recovery in canopy cover was generally rapid (5–6 years).

In contrast to many regions in Asia and Oceania, where mangroves are cleared for infrastructure development, agriculture or aquaculture, mangroves in Australia are protected by law, and approximately 19% are in IUCN recognized protected areas. Therefore, the observed gains and losses in mangrove extent are likely to be associated with environmental variability, and particularly to changes in the intensity of storms (tropical cyclones) and fluctuations in sea level. However, further research is required to quantify the role of specific causal mechanisms.

The analysis performed in this paper has been enabled by the data storage and processing capability provided by DEA and the fractional cover unmixing algorithm developed by the Joint Remote Sensing Research Program (JRSRP). This resource provides considerable opportunity to better understand the changing state of Australia's coastline given the capacity to map mangrove extent and change but also that of water inundation and the intertidal area with the ODC environment. A key interest is to use the DEA resource to better understand the observed responses of mangroves to sea level fluctuations and also tropical storms.

Acknowledgements

This paper published with permission of the CEO of Geoscience Australia. The authors would like to thank TERN AusCover and Geoscience Australia for providing funding to undertake the research and the Joint Remote Sensing Research Program. Jorg Hacker (Airborne Research Australia), Nicolas Goodwin (Queensland Department of Environment and Resource Management) and Adrian Fisher (University of Queensland) are also thanked for providing additional LiDAR datasets extending the geographical spread of the PCC% data. The European Regional Development Fund (ERDF) Ser Cymru program is also thanked. This research did not receive any specific grant from funding agencies in the public, commercial, or not-for-profit sectors.

References

Alongi, D.M., 2008. Mangrove forests: resilience, protection from tsunamis, and responses to global climate change. Estuar. Coast. Shelf Sci. 76, 1–13. https://doi.org/10.1016/j.ecss.2007.08.024.

Asbridge, E., Lucas, R.M., 2016. Mangrove response to environmental change in Kakadu National Park. IEEE Journal of Selected Topics in Applied Earth Observations and Remote Sensing 9, 5612–5620. https://doi.org/10.1109/JSTARS.2016.2616449.

Asbridge, E., Lucas, R., Ticehurst, C., Bunting, P., 2016. Mangrove response to environmental change in Australia's Gulf of Carpentaria. Ecol. Evol. 6, 3523–3539. https://doi.org/10.1002/ece3.2140.

Australian Government, 2013. Australian weather and seasons – a variety of climates. Australian Government 1–717. http://www.australia.gov.au/about-australia/australian-story/austn-weather-and-the-seasons.

Brocklehurst, P., Edmeades, B., 1996. Mangrove Survey of Darwin Harbour, Northern Territory (NT): CCNT/NFI Project 1994-95. Department of Lands Planning and Environment.

Bunting, P., Rosenqvist, A., Lucas, R., Rebelo, L.-M., Hilarides, L., Thomas, N., Hardy, A., Itoh, T., Shimada, M., Finlayson, M., 2018. The global mangrove watch—a new 2010 global baseline of mangrove extent. Remote Sens. 10 (10), 1669. https://doi.org/10.3390/rs10101669.

Bureau of Meteorology, 2016. Average annual & monthly maximum, minimum, & mean temperature. Australian Government, Bureau of Meteorologyhttp://www.bom.gov.au/jsp/ncc/climate_averages.

Chaudhuri, P., Ghosh, S., Bakshi, M., Bhattacharyya, S., Nath, B., 2015. A Review of Threats and Vulnerabilities to Mangrove Habitats: With Special Emphasis on East Coast of India. J. Earth Sci. Clim. Chang. 6, 1–9. https://doi.org/10.4172/2157-7617.1000270.

Congalton, R.G., 1991. A review of assessing the accuracy of classifications of remotely sensed data. Remote Sens. Environ. 37 (1), 35–46. https://doi.org/10.1016/F0034-4257(91)90048-B.

Cresswell, I.D., Semeniuk, V., 2011. Mangroves of the Kimberley coast: ecological patterns in a tropical ria coast setting. J. R. Soc. West. Aust. 94, 213–237.

Department of the Environment, 2016. Interim Biogeographic Regionalisation for Australia (Subregions - States and Territories). 7.

Duke, N.C., Kovacs, J.M., Griffiths, A.D., Preece, L., Hill, D.J.E., Oosterzee, P. van, Mackenzie, J., Morning, H.S., Burrows, D., 2017. Large-scale dieback of mangroves in Australia's Gulf of Carpentaria: a severe ecosystem response, coincidental with an unusually extreme weather event. Mar. Freshw. Res. 68, 1816–1829. https://doi.org/10.1071/MF16322.

Egbert, G.D., Erofeeva, S.Y., 2010. The OSU TOPEX/Poseiden Global Inverse Solution TPXO [WWW document]. TPXO8-atlas version 10. URL. http://volkov.oce.orst.edu/tides/global.html, Accessed date: 15 February 2016.

Ellison, A.M., Farnsworth, E.J., 1997. Simulated sea level change alters anatomy, physiology, growth, and reproduction of red mangrove (Rhizophora mangle L.). Oecologia 112, 435–446. https://doi.org/10.1007/s004420050330.

Fiala, A.C.S., Garman, S.L., Gray, A.N., 2006. Comparison of five canopy cover estimation techniques in the western Oregon Cascades. For. Ecol. Manag. 232, 188–197. https://doi.org/10.1016/j.foreco.2006.05.069.

Friess, D.A., 2016. Ecosystem services and disservices of mangrove forests: insights from historical colonial observations. Forests 7, 183. https://doi.org/10.3390/f7090183.

Furukawa, K., Wolanski, E., Mueller, H., 1997. Currents and sediment transport in mangrove forests. Estuarine, Coastal and Shelf Science 44, 301–310. https://doi.org/10.1006/ecss.1996.0120.

Gill, T., Johansen, K., Phinn, S., Trevithick, R., Scarth, P., Armston, J., 2017. A method for mapping Australian woody vegetation cover by linking continental-scale field data and long-term Landsat time series. International Journal of Remote Sensing 38, 679–705. https://doi.org/10.1080/01431161.2016.1266112.

Giri, C., Ochieng, E., Tieszen, L.L., Zhu, Z., Singh, A., Loveland, T., Masek, J., Duke, N., 2011. Status and distribution of mangrove forests of the world using earth observation satellite data. Global Ecology and Biogeography 20, 154–159. https://doi.org/10.1111/j.1466-8238.2010.00584.x.

Hay, T., Gribble, N., de Vries, C., Danaher, K., Dunning, M., Hearnden, M., Caley, P., Wright, C., Brown, I., Bailey, S., Phelan, M., 2005. Methods for Monitoring the Abundance and Habitat of the Northern Australian Mud Crab *Scylla serrata*. Project Report Fisheries Research & Development Corporation, pp. 138.

Irish, R.R., 2000. Landsat 7 automatic cloud cover assessment. pp. 348–355. doi:https://doi.org/10.1117/12.410358

Korhonen, L., Korhonen, K.T., Rautiainen, M., Stenberg, P., 2006. Estimation of forest canopy cover: a comparison of field measurement techniques.

Lewis, A., Oliver, S., Lymburner, L., Evans, B., Wyborn, L., Mueller, N., Raevksi, G., Hooke, J., Woodcock, R., Sixsmith, J., Wu, W., Tan, P., Li, F., Killough, B., Minchin, S., Roberts, D., Ayers, D., Bala, B., Dwyer, J., Dekker, A., Dhu, T., Hicks, A., Ip, A., Purss, M., Richards, C., Sagar, S., Trenham, C., Wang, P., Wang, L.-W., (2017) The Australian geoscience data cube — foundations and lessons learned. Remote Sensing of Environment. 202, 276-292doi:https://doi.org/10.1016/j.rse.2017.03.015

Li, F., Jupp, D.L.B., Reddy, S., Lymburner, L., Mueller, N., Tan, P., Islam, A., 2010. An evaluation of the use of atmospheric and BRDF correction to standardize landsat data. IEEE Journal of Selected Topics in Applied Earth Observations and Remote Sensing 3, 257–270. https://doi.org/10.1109/JSTARS.2010.2042281.

Lovelock, C.E., Feller, I.C., Reef, R., Hickey, S., Ball, M.C., 2017. Mangrove dieback during fluctuating sea levels. Sci. Rep. 7, 1680. https://doi.org/10.1038/s41598-017-01927-6.

Lucas, R., Rebelo, L.-M., Fatoyinbo, L., Rosenqvist, A., Itoh, T., Shimada, M., Simard, M., Souza-Filho, P.W., Thomas, N., Trettin, C., Accad, A., Carreiras, J., Hilarides, L., 2014. Contribution of L-band SAR to systematic global mangrove monitoring. Mar. Freshwater Res. 65, 589–603. https://doi.org/10.1071/MF13177.

Lucas, R., Finlayson, C.M., Bartolo, R., Rogers, K., Mitchell, A., Woodroffe, C.D., Asbridge, E., Ens, E., 2017. Historical perspectives on the mangroves of Kakadu National Park. Mar. Freshwater Res. https://doi.org/10.1071/MF17065.

Lugo, A.E., 2000. Effects and outcomes of Caribbean hurricanes in a climate change scenario. Science of The Total Environment, Climate change, Forests and 262, 243–251. https://doi.org/10.1016/S0048-9697(00)00526-X.

Luther, D.A., Greenberg, R., 2009. Mangroves: A Global Perspective on the Evolution and Conservation of Their Terrestrial Vertebrates. BioScience 59, 602–612. https://doi.org/10.1525/bio.2009.59.7.11.

Montreal Process Implementation Group for Australia and National Forest Inventory Steering Committee, 2013. Australia's State of the Forests Report 2013. ABARES, Canberra978-1-74323-169-2 December.

Mueller, N., Lewis, A., Roberts, D., Ring, S., Melrose, R., Sixsmith, J., Lymburner, L., McIntyre, A., Tan, P., Curnow, S., Ip, A., 2016. Water observations from space: mapping surface water from 25 years of Landsat imagery across Australia. Remote Sensing of Environment 174, 341–352. https://doi.org/10.1016/j.rse.2015.11.003.

Nardin, W., Locatelli, S., Pasquarella, V., Rulli, M.C., Woodcock, C.E., Fagherazzi, S., 2016. Dynamics of a fringe mangrove forest detected by Landsat images in the Mekong River Delta, Vietnam. Earth Surf. Process. Landforms 41, 2024–2037. https://doi.org/10.1002/esp.3968.

Neldner, V.J., Butler, D.W., Guymer, G.P., 2017. Queensland's Regional Ecosystems: Building and Maintaining a Biodiversity Inventory, Planning Framework and Information System for Queensland. Science Delivery Division, Department of Science, Information Technology and Innovation, PO Box 5078, Brisbane,

Queensland, 4001.
Olofsson, P., Foody, G.M., Stehman, S.V., Woodcock, C.E., 2013. Making better use of accuracy data in land change studies: estimating accuracy and area and quantifying uncertainty using stratified estimation. Remote Sensing of Environment 129, 122–131. https://doi.org/10.1016/j.rse.2012.10.031.
Osland, M.J., Feher, L.C., Griffith, K.T., Cavanaugh, K.C., Enwright, N.M., Day, R.H., Stagg, C.L., Krauss, K.W., Howard, R.J., Grace, J.B., Rogers, K., 2017. Climatic controls on the global distribution, abundance, and species richness of mangrove forests. Ecol Monogr 87, 341–359. https://doi.org/10.1002/ecm.1248.
Pedregosa, F., Varoquaux, G., Gramfort, A., Michel, V., Thirion, B., Grisel, O., Blondel, M., Prettenhofer, P., Weiss, R., Dubourg, V., Vanderplas, J., 2011. Scikit-learn: Machine learning in Python. J. Mach. Learn. Res. 12 (Oct), 2825–2830.
Peel, M.C., Finlayson, B.L., McMahon, T.A., 2007. Updated world map of the Köppen-Geiger climate classification. Hydrol. Earth Syst. Sci. 11, 1633–1644. https://doi.org/10.5194/hess-11-1633-2007.
Pontius Jr., R.G., Millones, M., 2011. Death to Kappa: birth of quantity disagreement and allocation disagreement for accuracy assessment. International Journal of Remote Sensing 32 (15), 4407–4429. https://doi.org/10.1080/01431161.2011.552923.
Ricklefs, R.E., Latham, R.E., 1993. Global Patterns of Diversity in Mangrove Floras. Species Diversity in Ecological Communities: Historical and Geographical Perspectives. University of Chicago Press, Chicago, pp. 215–229.
Roberts, D., Mueller, N., Mcintyre, A., 2017. High-dimensional pixel composites from earth observation time series. IEEE Transactions on Geoscience and Remote Sensing 55 (11), 6254–6264. https://doi.org/10.1109/TGRS.2017.2723896.
Rogers, K., Lymburner, L., Salum, R., Brooke, B.P., Woodroffe, C.D., 2017. Mapping of mangrove extent and zonation using high and low tide composites of Landsat data. Hydrobiologia 1–20. https://doi.org/10.1007/s10750-017-3257-5.
Romijn, E., Ainembabazi, J.H., Wijaya, A., Herold, M., Angelsen, A., Verchot, L., Murdiyarso, D., 2013. Exploring different forest definitions and their impact on developing REDD+ reference emission levels: a case study for Indonesia. Environmental Science & Policy 33, 246–259. https://doi.org/10.1016/j.envsci.2013.06.002.
Saenger, P., West, P.W., 2016. Determinants of some leaf characteristics of Australian mangroves. Bot J Linn Soc 180, 530–541. https://doi.org/10.1111/boj.12386.
Sagar, S., Roberts, D., Bala, B., Lymburner, L., 2017. Extracting the intertidal extent and topography of the Australian coastline from a 28 year time series of Landsat observations. Remote Sensing of Environment 195, 153–169. https://doi.org/10.1016/j.rse.2017.04.009.
Spalding, M.D, Blasco, F., Field, C.D. (Eds.) (1997). World Mangrove Atlas. Okinawa (Japan): International Society for Mangrove Ecosystems. 178 pp. Compiled by UNEP-WCMC, in collaboration with the International Society for Mangrove Ecosystems (ISME).
Spalding, M., Kainuma, M., Collins, L., 2010. World Atlas of Mangroves (Version 1.1). A Collaborative Project of ITTO, ISME, FAO, UNEP-WCMC, UNESCO-MAB, UNU-INWEH and TNC. Earthscan, London, London (UK) (319 pp).
Staben, G.W., Evans, K.G., 2008. Estimates of tree canopy loss as a result of Cyclone Monica, in the Magela Creek catchment northern Australia. Austral Ecology 33, 562–569. https://doi.org/10.1111/j.1442-9993.2008.01911.x.
Thomas, N., Lucas, R., Bunting, P., Hardy, A., Rosenqvist, A., Simard, M., 2017. Distribution and drivers of global mangrove forest change, 1996–2010. PLOS ONE 12, e0179302. https://doi.org/10.1371/journal.pone.0179302.
Thomas, N., Bunting, P., Lucas, R., Hardy, A., Rosenqvist, A., Fatoyinbo, T., 2018. Mapping mangrove extent and change: a globally applicable approach. Remote Sensing 10 (9), 1466. https://doi.org/10.3390/rs10091466.
Ward, R.D., Friess, D.A., Day, R.H., MacKenzie, R.A., 2016. Impacts of climate change on mangrove ecosystems: a region by region overview. Ecosyst Health Sustain 2, n/a-n/a. doi:https://doi.org/10.1002/ehs2.1211
Wells, A.G., 1983. Distribution of mangrove species in Australia, in: Biology and Ecology of Mangroves. Tasks for Vegetation Science. Springer, Dordrecht, pp. 57–76. https://doi.org/10.1007/978-94-017-0914-9_6.
Woodroffe, C.D., 1995. Response of tide-dominated mangrove shorelines in Northern Australia to anticipated sea-level rise. Earth Surf. Process. Landforms 20, 65–85. https://doi.org/10.1002/esp.3290200107.
Wulder, M.A., Masek, J.G., Cohen, W.B., Loveland, T.R., Woodcock, C.E., 2012. Opening the archive: how free data has enabled the science and monitoring promise of Landsat. Remote Sensing of Environment, Landsat Legacy Special Issue 122, 2–10. https://doi.org/10.1016/j.rse.2012.01.010.
Wulder, M.A., White, J.C., Loveland, T.R., Woodcock, C.E., Belward, A.S., Cohen, W.B., Fosnight, E.A., Shaw, J., Masek, J.G., Roy, D.P., 2016. The global Landsat archive: Status, consolidation, and direction. Remote Sens. Environ. 185, 271–283.
Zhu, Z., Woodcock, C.E., 2012. Object-based cloud and cloud shadow detection in Landsat imagery. Remote Sensing of Environment 118, 83–94. https://doi.org/10.1016/j.rse.2011.10.028.